# A Generalized Framework for Assessing Cargo Loss Impacts of Alternative Maritime Fuels

Danika Eamer[1,*], Stamatis Stamatelopoulos[1], Amr Y. Elbanhawy[2], Fotini Christia[1], Themistoklis Sapsis[1], Elsa Olivetti[1]

[1]Massachusetts Institute of Technology, Cambridge, MA, USA

[2]Energy Technology and Climate Change Laboratory, Department of Mechanical Engineering, Ain Shams University, Cairo, Egypt

[*]Corresponding author: danikam@mit.edu

**Abstract**

A generalized framework is presented to quantify cargo capacity losses and cost impacts of transitioning maritime vessels from conventional fuel oil to alternative fuels such as hydrogen, ammonia, methanol, and liquefied natural gas. Cargo loss is primarily governed by the tank-to-cargo capacity ratio, with smaller vessels experiencing substantially larger penalties than larger vessels. Boil-off gas losses introduce nonlinear cargo penalties for cryogenic fuels but remain modest (under 10%) under expected reliquefaction conditions. U.S. import and export cargoes are largely volume-limited, making low-density fuels such as hydrogen especially costly in terms of displaced cargo. Ammonia and methanol exhibit near-linear cargo losses with respect to the tank-to-cargo capacity ratio, with volume losses of 3–16% for representative vessels, while liquefied hydrogen and natural gas show wider variation due to boil-off losses and pilot tank size. Cargo capacity losses can exceed 30% for compressed and liquefied hydrogen, and transport costs can increase by over 50% for small vessels. Compressed hydrogen incurs the highest cost increase (21–112%), while cargo penalties increase costs by only 3–12% for methanol and LNG. These results highlight the importance of cargo- and vessel-specific analysis in maritime decarbonization strategies and the need to incorporate cargo loss into fuel transition planning and techno-economic assessments.

**Keywords:** Maritime shipping, Alternative fuels, Cargo loss, Vessel design, Boil-off gas, Stowage factor

# 1 Introduction

Maritime shipping is the backbone of the global economy, transporting more than 80% of all international trade and, in doing so, producing roughly 3% of anthropogenic greenhouse gas (GHG) emissions (International Maritime Organization, 2021). In 2023, the International Maritime Organization (IMO) adopted a strategy that calls for net-zero lifecycle GHG emissions from ships "by or around 2050" (International Maritime Organization, 2023). These ambitions have intensified interest in low- and zero-carbon fuels − ammonia, hydrogen, methanol, liquefied natural gas (LNG), and others − that offer potential for substantial well-to-wake emission reductions relative to the fuel oil and marine diesel conventionally used for maritime applications.

Most candidate alternative fuels have far lower energy densities than fuel oil or marine diesel, whose high energy density enables deep-sea vessels to complete cross-continental roundtrips with minimal loss of cargo space to fuel tanks. Cryogenic liquid fuels such as liquefied hydrogen ($LH_2$) and LNG further suffer evaporative (boil-off) losses that must be controlled through reliquefaction or venting. Collectively, these factors make fuel-storage requirements a first-order constraint in vessel design. Enlarged or additional tanks can physically displace payload or increase dead-weight tonnage, eroding cargo transport cost and revenue. Consequently, any rigorous assessment of alternative fuels must evaluate not only their emissions benefits and cost competitiveness, but also their implications for cargo-carrying capacity.

A growing body of research has estimated the tank-volume penalties and associated capacity losses for specific vessel-fuel combinations. These studies have shown that, depending on the fuel and trading pattern, cargo space losses can range from negligible to double-digit percentages and may lead to substantial increases in levelized transport costs (Kim et al., 2020; Horvath et al., 2018; Korberg et al., 2021; Stolz et al., 2022). However, three critical gaps remain. First, existing studies typically focus on specific vessels and applications − such as a single ship class or design range − without offering a generalized framework to compare cargo loss across diverse vessel designs and fuel choices. As a result, they provide limited insight into how differences in vessel class or size influence the cargo displacement. Second, although several authors quantify daily boil-off rates, few propagate these rates into revised tank-size requirements or compare boil-off gas (BOG) impacts systematically across fuels. Third, existing work rarely accounts for the fact that whether a vessel is ultimately mass-limited or volume-limited depends on the stowage factor of the commodity carried; capacity penalties should in general be evaluated with respect to effective cargo limits that account for this commodity-specific constraint.

This study makes four key contributions. First, an analytical framework is developed that clearly sep-

arates fuel properties from vessel design and operational choices, enabling a generalized assessment of how vessel design choices influence cargo loss across alternative fuels. This framework is further evaluated numerically using Monte Carlo sampling to assess the sensitivity of cargo loss to vessel design parameters for vessels operating on $LH_2$, compressed hydrogen ($CH_2$), liquified ammonia, methanol, and liquefied natural gas (LNG). Results for representative bulk carrier, container, tanker, and gas carrier vessels defined in the NavigaTE maritime shipping model (Hintze et al., 2023) are compared to randomly sampled vessel configurations, allowing key design constraints and correlations that shape real-world outcomes to be identified. Second, conventional tank-scaling approaches are extended by introducing a boil-off correction factor that links BOG loss and reliquefaction energy directly to cargo displacement. Third, real-world cargo densities are explicitly incorporated using stowage factors drawn from U.S. commodity flow data, enabling classification of each vessel and cargo as mass- or volume-constrained. Lastly, by coupling these physical drivers to capital, operating, and fuel costs, the analysis translates capacity penalties into cost-per-tonne-mile metrics for ten representative vessel types within the NavigaTE fleet model, providing a fleet-wide economic signal for operators and policy-makers.

The remainder of the paper is organized as follows. Section 2 reviews prior work on cargo displacement and cryogenic liquified fuel storage, establishing the context for this work. Section 3 presents the analytical framework, the treatment of boil-off and reliquefaction, and the integration with commodity-specific stowage factors and fleet-level trade data. Section 4 quantifies tank-scaling penalties across fuels, maps mass- versus volume-limited regimes, and examines how these physical constraints propagate to transport cost impacts.

# 2 Literature Review

This section first reviews prior work to quantify and assess impacts of cargo capacity losses resulting from the use of alternative shipping fuels. This is followed by a brief review of work both within and beyond the maritime sector on storage requirements and BOG rates of cryogenic liquefied fuels.

## 2.1 Quantifying and accounting for cargo losses

A number of academic studies have examined how the use of alternative fuels affects cargo capacity across different vessel types. Kim et al. (2020) estimated increases in tank mass and volume of up to 130% and 60%, respectively, for a 2,500 TEU container vessel transitioning to ammonia fuel, accounting for the full propulsion system and tank arrangement in various propulsion system configurations. Horvath et al. (2018) quantified cargo volume losses up to 13% for $LH_2$, 5% for methanol, and 2.5% for LNG, based on energy conversion efficiency and fuel energy density. These losses translated into levelized cost of mobility increases

of up to 15% for $LH_2$. Korberg et al. (2021) found that reduced cargo space added less than 5% to the total cost of ownership for vessels using methanol.

Stolz et al. (2022) assessed the fraction of Europe's bulk cargo shipping that could be maintained under alternative fuels, allowing up to 3% cargo capacity loss. Over 90% of current routes were found to be viable with $CH_2$, ammonia, methanol, and LNG. A 2020 study by the International Council for Clean Transportation (Mao et al., 2020) performed a similar analysis of transpacific container routes, finding that 43% of China-US voyages could be completed on $LH_2$ without cargo loss, rising to nearly 100% if up to 5% cargo displacement is permitted. An LNG-specific study by marine classification society Germanischer Lloyd estimated approximately 3% volume loss for medium-sized container ships (Andersen et al., 2013).

A series of applied studies by the Mærsk Mc-Kinney Møller Center for Zero Carbon Shipping (MMMCZCS) provide more detailed evaluations of cargo displacement under specific vessel designs and operational ranges. A concept study for a 3,500 TEU ammonia-fueled container vessel found that cargo losses could be limited to 1% (128 TEU) with strategic tank placement using either prismatic or type C tanks (MMMCZCS, 2025). A corresponding design for a 15,000 TEU container ship proposed placing tanks beneath accommodations to avoid cargo bay intrusion, though quantitative losses were not specified (MMMCZCS, 2023).

In a more comprehensive study, MMMCZCS (2024a) examined ship design principles for ammonia adoption, evaluating tank placement both above deck and within cargo holds. For a capesize bulk carrier, using ammonia to match a 10,000 nautical mile (nm) range led to a 2.4% DWT loss, while allowing for a shorter 5,000 nm range resulted in only 0.6% loss. Similar analyses were conducted for tanker retrofits (MMMCZCS, 2024b), where above-deck methanol tanks on small Long Range 2 tankers enabled full volume cargo capacity, while Very Large Crude Carriers required below-deck storage that displaced up to 12,000 $m^3$ of cargo volume to preserve range. Reducing the design range to 14,000-15,000 nm enabled above-deck tank storage and avoided cargo displacement. For container vessels, MMMCZCS (2022) estimated that full-range ammonia retrofits (12,000 nm) displaced 1,100 TEU (7%), whereas shorter-range conversions (7,000 nm) limited the loss to 400 TEU (3%). For methanol, 2-3% losses (240-400 TEU) were typical. These design studies underscore the key role of tank placement and acceptable range reduction in mitigating cargo loss for alternative fuels.

## 2.2 Storage of liquefied fuels

Storing liquefied fuels introduces engineering challenges due to their cryogenic or high-pressure requirements. Hydrogen, with a boiling point of -253°C, is particularly demanding (Rivard et al., 2019). To limit heat

ingress and subsequent BOG generation, liquefied fuels are typically stored in spherical or cylindrical type C tanks with polyurethane foam or vacuum insulation (Klell, 2010; International Maritime Organization, 2016; Demharter, 1998). These configurations are common in LNG vessels and assumed in conceptual $LH_2$ vessel designs (Ahn et al., 2017; Alkhaledi et al., 2022; Klebanoff et al., 2017; American Bureau of Shipping, 2021).

BOG generation can be amplified by sloshing during transit, which increases kinetic energy transfer and evaporation rates. Smith et al. (2022) estimate that sloshing can increase BOG rates by up to 4% for LNG and 8% for $LH_2$. While BOG can be utilized for propulsion at sea (Krikkis, 2018), port operations require reliquefaction or venting. First introduced in 2000 aboard the Jamal LNG carrier (Gómez et al., 2013), the practice of reliquefying BOG is now standard for LNG, with modern systems achieving energy requirements for reliquefaction, referred to as "specific energy consumption" (SEC), as low as 0.59 kWh/kg (Wärtsilä, 2020).

For liquefied ammonia and hydrogen as maritime fuels, such systems remain conceptual. Choi et al. (2025) simulated a $LH_2$ reliquefaction system using $LH_2$ as a refrigerant, achieving a SEC of 5.03 kWh/kg. Ji et al. (2025) compared options for ammonia BOG reliquefaction, finding that a Linde-Hampson cycle achieved a SEC of 0.17 kWh/kg.

These storage challenges, particularly boil-off losses and the need for energy-intensive reliquefaction, represent important vessel and tank design considerations, as they directly impact tank sizing and cargo displacement.

# 3 Theory and Calculation

## 3.1 Vessel Model

Cargo losses of real-world vessels operating on alternative fuels are compared using the NavigaTE fleet model developed by the Mærsk Mc-Kinney Møller Center for Zero Carbon Shipping (MMMCZCS) (Hintze et al., 2023). Vessel design specifications, informed by input from MMMCZCS industry partners, define internal combustion engine powertrains compatible with a range of conventional and alternative fuels across representative bulk carriers, container ships, tankers, and gas carriers. The model also simulates operating costs and emissions for each fuel-vessel combination using methods detailed in Eamer et al. (2025a) and Section 3.6.

The following alternative maritime fuels are considered in this work: hydrogen, ammonia, methane, and methanol. Ammonia is assumed to be cryogenically stored in liquid form at its boiling point of -33°C

(Rumble, 2025). Hydrogen is assumed to be stored either in cryogenic liquid form ($LH_2$) by cooling it to its boiling point of -253°C (Rumble, 2025), or compressed to 700 bar ($CH_2$). Table F.1 summarizes the physical properties of these fuels used in this work. It is assumed that powertrains equipped to use any alternative fuel will also support the use of conventional fuel oil, and are hence referred to as "dual fuel" powertrains. This is in part because it is expected that these alternative powertrains will initially require some minimum fraction of their energy to come from conventional fuel oil, which is referred to in this context as "pilot fuel". As a result, dual fuel vessels are modeled with two separate tanks to contain the alternative and pilot fuels.

The cargo capacities of bulk carrier and tanker vessels are measured by mass, whereas container ships and gas carriers are measured by volume. Table 1 summarizes the tank size and cargo capacity of each vessel considered in this work operating on conventional fuel oil − referred to as the "nominal" tank size and capacity − along with the assumed pilot fuel tank size for dual fuel powertrains. Tables F.2 and F.3 detail additional specifications used to define each vessel and powertrain considered. All NavigaTE model inputs used in this work (using version 2 defaults time stamped on June 18, 2025) can also be found in Eamer et al. (2025b).

| **Vessel Class** | **Size Label** | **Nominal Cargo Capacity** ($m_o^{\text{cargo}}$ or $V_o^{\text{cargo}}$) | **Nominal Fuel Tank Size** $V_o^{\text{tank}}$ **(m$^3$)** | **Pilot Fuel Tank Size** $V^{\text{tank, pilot}}$ **(m$^3$)** | **Pilot fuel tank size ratio f$_p$** |
|---|---|---|---|---|---|
| Bulk Carrier | Capesize | 200k tonnes | 5000 | 500 | 0.1 |
| | Pamanax | 75k tonnes | 3000 | 500 | 0.117 |
| | Handy | 35k tonnes | 2000 | 500 | 0.25 |
| Tanker | 300k DWT | 300k tonnes | 8000 | 1500 | 0.188 |
| | 100k DWT | 100k tonnes | 3000 | 500 | 0.167 |
| | 35k DWT | 35k tonnes | 2000 | 500 | 0.25 |
| Container Ship | 15,000 TEU | 574k m$^3$ | 15000 | 4000 | 0.267 |
| | 8,000 TEU | 306k m$^3$ | 9000 | 2000 | 0.222 |
| | 3,500 TEU | 134k m$^3$ | 3500 | 1000 | 0.286 |
| Gas carrier | 100k m$^3$ | 100k m$^3$ | 2000 | 500 | 0.25 |

Table 1: Capacity estimates for each vessel modeled. TEU, which stands for "twenty-foot equivalent units", is a standard volumetric measure of cargo capacity for container ships. Similarly, DWT, which stands for "deadweight tonnes" is a standard measure of mass-carrying capacity for bulk carriers and tankers. m$^3$ stands for "cubic meters", a standard capacity measure for gas carriers. Source: NavigaTE version 2 defaults time stamped on June 18, 2025 (Eamer et al., 2025b).

## 3.2 Tank Capacity Scaling

To enable a direct comparison of cargo losses between alternative fuel options for a given vessel, it is assumed that each fuel will require sufficiently large alternative fuel tanks to achieve the same design range as a

conventional fuel oil vessel, ultimately without the use of pilot fuel.

The design range $R_f$ of a vessel operating on fuel $f$ is defined as the distance, in nautical miles, that the vessel can cover at sea on a single tank of fuel. The design range can be expressed in terms of vessel design and fuel parameters as follows (derivation in Appendix A):

$$R_f = \frac{(\text{LHV})_f \eta_f m_f^{\text{tank}} s^{\text{av}}}{f_f^{\text{boil-off}} P^{\text{av}}} = \frac{(\text{LHV})_f \eta_f \rho_f V_f^{\text{tank}} s^{\text{av}}}{f_f^{\text{boil-off}} P^{\text{av}}} \tag{1}$$

where $(\text{LHV})_f$ is the fuel's lower heating value, $\rho_f$ is its mass density, and $V_f$ and $m_f = \rho_f V_f$ are the volume and mass capacities, respectively, of the main fuel tank. The average speed $s^{\text{av}}$ and the average combined power demand $P^{\text{av}}$ of the vessel's electrical, heat and propulsion systems are evaluated over all operating conditions, as detailed in Appendix A. $\eta_f$ is the overall efficiency with which the fuel's energy is converted into mechanical propulsion by the vessel's powertrain, accounting for losses to the electrical and heat systems. Appendix B shows how $\eta_f$ is evaluated based on the efficiencies and power requirements of the vessel's main propulsion, electrical, and heat systems, along with the fraction of time at sea. The boil-off factor $f_f^{\text{boil-off}} \geq 1$ accounts for the increase in tank capacity needed to compensate for additional fuel used to reliquefy BOG while the vessel is at port, assuming the BOG is used for propulsion while at sea.

Letting $V_o^{\text{tank}}$ denote the fuel tank volume needed to achieve a vessel design range $R_o$ for a conventional fuel oil vessel, the volume capacity $V_f^{\text{tank}}$ of an alternative tank needed to maintain constant $R_o$ is given by:

$$V_f^{\text{tank}} = f_f^{\text{density, V}} f_f^{\text{eff}} f_f^{\text{boil-off}} V_o^{\text{tank}} \tag{2}$$

and the required mass capacity $m_f^{\text{tank}}$ is given by:

$$m_f = f_f^{\text{density, m}} f_f^{\text{eff}} f_f^{\text{boil-off}} m_o^{\text{tank}} \tag{3}$$

where $f_f^{\text{density, V}} = \frac{(\text{LHV})_o \rho_o}{(\text{LHV})_f \rho_f}$ and $f_f^{\text{density, m}} = \frac{(\text{LHV})_o}{(\text{LHV})_f}$ are intrinsic to the alternative fuel, and account for the alternative fuel's mass and energy density. $f_f^{\text{eff}} = \frac{\eta_o}{\eta_f}$ accounts for the overall efficiency of the vessel's conversion systems and $f_f^{\text{boil-off}}$ accounts for boil-off losses; both depend on the vessel's energy conversion systems, power requirements, and operational characteristics.

### 3.2.1 Boil-off Gas and Reliquefaction

For liquefied fuels such as $LH_2$, LNG, and ammonia, boil-off gas (BOG) is modeled as a constant daily mass loss fraction $r_f^{\text{boil-off}}$ of the remaining onboard fuel. For $LH_2$, a conservative value of $r_{\text{LH2}}^{\text{boil-off}} = 0.5\%/\text{day}$ is used, reflecting reported ranges of 0.2-0.4%/day from insulated tank studies (Abe et al., 1998) and up

to 0.62%/day when accounting for sloshing-induced evaporation (Smith et al., 2022). For LNG, a rate of 0.1%/day is adopted, based on reported performance for the EKAPUTRA LNG carrier (Wärtsilä, 2025). Liquid ammonia is assumed to lose fuel at 0.03%/day, consistent with published values between 0.02–0.04%/day (Morgan, 2013; Al-Breiki et al., 2020). While BOG can be used for propulsion at sea, fuel lost at port must be reliquefied and returned to storage, with assumed SECs drawn from the literature introduced in Section 2.2 and summarized in Table 4.

To account for the additional fuel burn needed to power the reliquefaction process, an effective rate of fuel loss, $r_f^{\text{boil-off, eff}}$, is calculated as:

$$r_f^{\text{boil-off, eff}} = \frac{r_f^{\text{boil-off}} \times (\text{SEC})_f}{\eta^{\text{elec}} \times (\text{LHV})_f} \tag{4}$$

where $\eta^{\text{elec}}$ is the efficiency with which fuel energy is converted to onboard electrical power, assumed to be 48% for all alternative fuels (see Table F.3).

Assuming the vessel fully empties its tank before refueling and would lose fuel at an average daily rate of $\frac{m_f}{N}$ in the absence of boil-off, the mass of fuel in the vessel's tank would need to be scaled up by the following factor, derived in Appendix C, to correct for losses from fuel boil-off and reliquefaction.

$$f_f^{\text{boil-off}} = \left( \frac{1}{(1 - r_f^{\text{boil-off, eff}})^{f^{\text{port}} N}} \right) \cdot \left( \frac{1}{N} \frac{1 - (1 - r_f^{\text{boil-off, eff}})^{f^{\text{port}} N}}{1 - (1 - r_f^{\text{boil-off, eff}})^{f^{\text{port}}}} \right) \tag{5}$$

where $f^{\text{port}} = 1 - f^{\text{sea}}$ is the average fraction of time the vessel spends at port. Lacking detailed knowledge of when a given vessel will be at port as it empties its tank − during which time BOG must be reliquefied rather than used for propulsion − Equation 5 makes a simplifying assumption that a vessel's probability of being at port is uniformly distributed over the period it takes to empty its tank. While alternative distributions can be considered, they will in general not evaluate to a closed-form solution, requiring instead numerical evaluation of a product and sum of two geometric series, as shown in Appendix C.

With this assumption, the first term $\frac{1}{(1-r_f^{\text{boil-off, eff}})^{f^{\text{port}} N}}$ accounts for daily loss to boil-off in the absence of fuel draw by the vessel's power systems, and the second term $\frac{1}{N} \frac{1-(1-r_f^{\text{boil-off, eff}})^{f^{\text{port}} N}}{1-(1-r_f^{\text{boil-off, eff}})^{f^{\text{port}}}}$ corrects for the daily fuel draw of $\frac{m_f^{\text{tank, no boil-off}}}{N}$ to account for a continuous reduction in the amount of fuel available in the tank to be lost to boil-off.

The number of days $N$ to empty the tank is given by:

$$N = \frac{R}{s^{\text{av}} t^{\text{day}}} = \frac{(\text{LHV})_o \eta_o \rho_o V_o^{\text{tank}}}{P^{\text{av}} t^{\text{day}}} \tag{6}$$

where $t^{\text{day}}$ is the time elapsed per day.

## 3.3 Cargo Loss Impact

As a first-order approximation, the amount of cargo displaced by shifting to an alternative fuel from conventional fuel oil is assumed to be equal to the additional fuel tank capacity needed to maintain the same design range with the alternative fuel, using the scaling factors evaluated in Section 3.2. This approximation neglects added space demands that may arise from factors such as non-conformal tank shapes, added tank material for cryogenic or high-pressure fuel storage, related auxiliary systems, or added components that may be needed to support onboard crew safety with alternative fuels. It also neglects the possibility that vessel design ranges could be reduced when transitioning to alternative fuels by allowing for more frequent refueling stops.

With the above assumption, the cargo volume $V_f^{\text{cargo}}$ available on a dual fuel vessel operating with alternative fuel $f$ is obtained from the original cargo volume $V_o^{\text{cargo}}$ based on the added volume $V_f^{\text{tank}} - V_o^{\text{tank}}$ of the alternative fuel tank, and accounting for the added volume $V^{\text{tank, pilot}}$ of the pilot fuel oil tank:

$$V_f^{\text{cargo}} = V_o^{\text{cargo}} - (V_f^{\text{tank}} + V^{\text{tank, pilot}} - V_o^{\text{tank}}) \tag{7}$$

The relative cargo volume lost, $CL_f^{\text{volume}}$, in transitioning from a conventional fuel oil vessel to a dual fuel vessel with main fuel $f$ can then be expressed in terms of vessel design and tank scaling parameters by re-arranging Equation 7 and inserting Equation 2 for $V_f^{\text{tank}}$:

$$\text{CL}_f^{\text{volume}} = \frac{V_o^{\text{cargo}} - V_f^{\text{cargo}}}{V_o^{\text{cargo}}} = \frac{V_o^{\text{tank}}}{V_o^{\text{cargo}}}(f_f^{\text{density, V}} f_f^{\text{eff}} f_f^{\text{boil-off}} + f^{\text{pilot}} - 1) \tag{8}$$

where $f^{\text{pilot}} = \frac{V^{\text{tank, pilot}}}{V_o^{\text{tank}}}$ is the ratio of the pilot fuel oil tank size in dual fuel vessel to the main fuel tank size $V_o^{\text{tank}}$ in a conventional fuel oil vessel.

$V_f^{\text{cargo}}$ and $\text{CL}_f^{\text{mass}}$ are likewise obtained by substituting V→m in Equations 7 and 8.

## 3.4 Impact of Vessel Design Parameters on Cargo Loss

This section investigates the impact of varying vessel design parameters, summarized in Table 9, on the cargo loss.

### 3.4.1 Dimensionless Parameter Formulation

The fractional cargo loss in Equation 8 can be expressed in terms of dimensionless parameters as follows:

$$\text{CL}_f^{\text{volume}} = \alpha^{\text{volume}}(\beta_f^{\text{volume}} f_f^{\text{boil-off}} + f^{\text{pilot}} - 1) \tag{9}$$

$$\mathrm{CL}_f^{\mathrm{mass}} = \alpha^{\mathrm{mass}}(\beta_f^{\mathrm{mass}} f_f^{\text{boil-off}} + f^{\mathrm{pilot}} - 1) \tag{10}$$

The "fuel-independent" terms $\alpha^{\mathrm{volume}}$ and $\alpha^{\mathrm{mass}}$ are defined as the ratio of main tank size to cargo capacity for a vessel running on conventional fuel oil and, from Equations 1 and 6, scale with the vessel's design range and average power over speed $\frac{P^{\mathrm{av}}}{s^{\mathrm{av}}}$, or equivalently with the product $NP^{\mathrm{av}}$ of the average power and days to empty the tank:

$$\alpha^{\mathrm{mass}} = \frac{m_o^{\mathrm{tank}}}{m_o^{\mathrm{cargo}}} = \frac{R}{(\mathrm{LHV})_o \eta_o m_o^{\mathrm{cargo}}} \frac{P^{\mathrm{av}}}{s^{\mathrm{av}}} = NP^{\mathrm{av}} \frac{t^{\mathrm{day}}}{(\mathrm{LHV})_o \eta_o m_o^{\mathrm{cargo}}} \tag{11}$$

$$\alpha^{\mathrm{volume}} = \frac{V_o^{\mathrm{tank}}}{V_o^{\mathrm{cargo}}} = NP^{\mathrm{av}} \frac{t^{\mathrm{day}}}{(\mathrm{LHV})_o \eta_o \rho_o V_o^{\mathrm{cargo}}} \tag{12}$$

Increasing the $\alpha$ term by, for example, increasing the vessel's design range or reducing its nominal cargo capacity proportionally increases the relative cargo loss from transitioning to alternative fuels by amplifying the impact of further scaling up the tank size to accommodate an alternative fuel.

The "fuel-dependent" terms $\beta_f^{\mathrm{m}}$ and $\beta_f^{\mathrm{V}}$ scale the mass and volume, respectively, of a conventional fuel oil tank such that the vessel's energy conversion systems can output an equivalent amount of energy when operating with an alternative fuel $f$:

$$\beta_f^{\mathrm{m}} = f_f^{\text{density, m}} f_f^{\mathrm{eff}} = \frac{(\mathrm{LHV})_o \eta_o}{(\mathrm{LHV})_f \eta_f} \tag{13}$$

$$\beta_f^{\mathrm{V}} = f_f^{\text{density, V}} f_f^{\mathrm{eff}} = \frac{(\mathrm{LHV})_o \eta_o \rho_o}{(\mathrm{LHV})_f \eta_f \rho_f} \tag{14}$$

While the efficiencies $\eta_f$ and $\eta_o$ may be tweaked somewhat via design choices and can be expected to improve over time, $\beta_f^{\mathrm{m}}$ and $\beta_f^{\mathrm{V}}$ are assumed for this work to be fixed for a given alternative fuel $f$, and independent of vessel design parameters.

#### 3.4.2 Numerical Analysis with Monte Carlo

In general, choices of vessel design parameter values for real-world vessels are expected to exhibit some correlations arising from physical and economic constraints or optimizations. As the vessels defined in the NavigaTE model are designed to represent classes of real-world vessels, they should exhibit similar correlations to what would be seen in real-world vessels.

To distinguish effects of these real-world parameter choice correlations from general trends arising from

the mathematical relationships developed in Section 3.3, cargo loss results for vessels defined in NavigaTE are overlaid on 50,000 results for random sets of the six independent vessel design parameters listed in Table 2 are generated using the MC method (Mooney, 1997). For a given MC sample, the value of each parameter is randomly selected from a uniform distribution. The upper and lower bounds of the uniform distribution for a given parameter are set to its maximum and minimum values, respectively, over all vessels defined in NavigaTE. Table 2 summarizes the independent vessel design parameters varied in the MC analysis, along with their maximum and minimum values from Tables 1 and F.2.

| **Parameter** | **Minimum** | **Maximum** |
|---|---|---|
| $R$ | 17,710 nm | 50,510 nm |
| $\left(\frac{P}{s}\right)^{\text{av}}$ | 1,046 MJ/nm | 5,998 MJ/nm |
| $P^{\text{av}}$ | 3.3 MW | 31 MW |
| $f^{\text{pilot}}$ | 0.1 | 0.286 |
| $f^{\text{port}}$ | 0.179 | 0.5 |
| $V_o^{\text{cargo}}$ | 30,000 $\text{m}^3$ | 574,200 $\text{m}^3$ |
| $m_o^{\text{cargo}}$ | 35,000 tonnes | 423,000 tonnes |

Table 2: Summary of independent parameters varied randomly to generate sets of MC samples, along with their minimum and maximum values over all vessels defined in NavigaTE. Parameters are listed using their shorthand names defined in Table 9. The abbreviation "nm" represents "nautical miles."

### 3.4.3 Estimating non-default cargo capacities

As discussed in Section 3.1, cargo capacity is by default measured by mass for bulk carriers and tankers and by volume for container ships and gas carriers. In order to simultaneously evaluate mass and volume capacity losses for a given vessel class and size, Table 3 summarizes the approach used to estimate volume capacities of vessels whose capacity is measured by mass, and vice versa for vessels whose capacity is measured by volume.

| Vessel class | Default capacity measure | Alternate capacity measure | Approach used to estimate alternate capacity measure |
|---|---|---|---|
| Bulk carrier | Mass | Volume | For the Panamax and Handy sizes, volume capacity is obtained from the central value of the range provided by Maritime Brokers and Consultants, Inc. (2024). For the Capesize, the volume capacity is obtained from the mass capacity assuming a cargo density of 1 $m^3$ / tonne, based on the observation that the volume capacities estimated for Panamax and Handy sizes, in $m^3$, are close to their mass capacities in tonnes (+24%, −14%), see Table 6. |
| Tanker | Mass | Volume | The volume capacity is obtained from the mass capacity based on the density of light crude oil, 0.850 tonnes/$m^3$ (Alberta Energy Regulator, 2024). |
| Container ship | Volume | Mass | The mass capacity is obtained from the volume capacity based on the maximum allowed mass, 28,180 kg (Dedola Global Logistics, 2023), of a shipping container. |
| Gas carrier | Volume | Mass | The mass capacity is obtained from the volume capacity based on the density of LNG, 0.428 kg/L (U.S. Department of Energy, 2013). |

Table 3: Approaches used to estimate alternate capacity measures for vessels defined in NavigaTE.

### 3.5 Using stowage factor to evaluate effective capacity and cargo loss

A vessel's stowage factor (SF), expressed in $m^3$/tonne, is defined as the inverse density $\rho^{\text{cargo}}$ of cargo carried by the vessel:

$$\text{SF} = \frac{1}{\rho^{\text{cargo}}} \tag{15}$$

Cargo with relatively low SF is composed of high-density material(s) such as iron ore with $S \approx 0.5$ $m^3$/tonne (BMT, 2025), and high-SF cargo of low-density material(s) such as tobacco products with $S \approx 3.5$ (Freight Chartering Operations, 2015).

SF is used in this work to evaluate a vessel's effective cargo carrying capacity and cargo loss, depending on whether the capacity is mass- or volume-limited. The effective mass-carrying capacity $m^{\text{eff}}$ is determined as the smaller of two values: the vessel's nominal mass capacity $m_o^{\text{cargo}}$ (reduced by cargo losses $\text{CL}_f$ if alternative fuels are used) and its nominal volume capacity $V_c$ (adjusted for tank losses and converted to

mass using its SF).

$$m_{f,\mathrm{SF}}^{\text{cargo, eff}} = \min\left\{ \frac{V_o^{\text{cargo}}(1 - \mathrm{CL}_f^{\text{volume}})}{\mathrm{SF}},\ m_o^{\text{cargo}}(1 - \mathrm{CL}_f^{\text{mass}}) \right\} \tag{16}$$

and similarly, the effective volume capacity $V_{f,\mathrm{SF}}^{\text{eff}}$ is evaluated as:

$$V_{f,\mathrm{SF}}^{\text{cargo, eff}} = \min\left\{ \mathrm{SF} \cdot m_o^{\text{cargo}}(1 - \mathrm{CL}_f^{\text{mass}}),\ V_o^{\text{cargo}}(1 - \mathrm{CL}_f^{\text{volume}}) \right\} \tag{17}$$

The resulting effective cargo loss is equivalent for both mass and volume of cargo, and given by:

$$\mathrm{CL}_{f,\mathrm{SF}}^{\text{cargo, eff}} = \frac{m_{f,\mathrm{SF}}^{\text{cargo, eff}} - m_{o,\mathrm{SF}}^{\text{cargo, eff}}}{m_{o,\mathrm{SF}}^{\text{cargo, eff}}} = \frac{V_{f,\mathrm{SF}}^{\text{cargo, eff}} - V_{o,\mathrm{SF}}^{\text{cargo, eff}}}{V_{o,\mathrm{SF}}^{\text{cargo, eff}}} \tag{18}$$

The following section applies the methods developed in this section to evaluate effective cargo capacity and loss for vessels carrying U.S. import and export commodities.

### 3.5.1 Evaluating stowage factor ranges for U.S. import and export commodities

Bulk carriers and tankers generally carry commodities in "bulk", meaning that a single type of commodity $C$ is loaded onto the vessel for a given voyage. For these bulk vessels, the average effective volume capacity of a given vessel type − bulk carrier or tanker − is evaluated by calculating the effective volume capacity of a shipment carrying each commodity assumed to be carried by the given vessel type based on the commodity's SF, and weighting the contribution from each commodity by its relative annual import and export flow:

$$V_f^{\text{cargo, eff, av, bulk}} = \frac{\sum_i V_{f,\mathrm{SF}_{C_i}}^{\text{cargo, eff}} T_{C_i}}{\sum_i T_{C_i}} \tag{19}$$

where $i$ iterates over all commodities $C$ assumed to be carried by the given vessel type, $\mathrm{SF}_C$ represents the stowage factor of commodity $C$, and the annual trade flow $T_C$ represents the annual tonne-miles of commodity $C$ imported to or exported from U.S. ports. The effective mass capacity is similarly obtained by substituting V→m in Equation 19. Tonne-mile weights are applied as a proxy for voyage frequency due to data limitations; this simplification is found not to substantially influence the resulting SF-weighted averages.

Thanks to the modularity enabled by shipping containers, container ships generally carry multiple types of commodity per voyage. To account for this, the average effective volume capacity of containers is instead evaluated using the average SF, denoted $\mathrm{SF}^{\text{av}}$, of commodities assumed to be carried by container ships:

$$V_f^{\text{cargo, eff, av, container}} = V_{f,\mathrm{SF}^{\text{av}}}^{\text{cargo, eff}} \tag{20}$$

where the average SF is similarly obtained by weighting each commodity's SF by its annual trade flow:

$$\mathrm{SF}^{\mathrm{av}} = \frac{\sum_i \mathrm{SF}_{C_i} T_{C_i}}{\sum_i T_{C_i}} \tag{21}$$

Annual trade flows are obtained for 48 commodity categories carried by bulk carriers and container ships, using the U.S. Freight Analysis Framework version 5.6.1 (FAF5) database (Federal Highway Administration, 2025) and filtering for foreign imports and exports carried by sea. Table D.1 summarizes the information from the FAF5 data used in this work. Upper and lower SF bounds $[\mathrm{SF}_C^{\mathrm{lower}}, \mathrm{SF}_C^{\mathrm{upper}}]$ are estimated for each commodity assumed to be carried by bulk carriers and container ships from a range of public sources. These SF bounds are tabulated in Tables D.2 and D.3, and visualized along with the annual trade flow of each commodity in Figures D.1 and D.2.

Fuels carried by tanker are categorized into gasoline, fuel oil, and crude petroleum, following the commodity categorizations adopted in the FAF5 database. SFs for gasoline and fuel oil of 1.33 $\mathrm{m}^3$/tonne and 1.01 $\mathrm{m}^3$/tonne, respectively are obtained from the GREET lifecycle assessment model (Argonne National Laboratory, 2024) based on their typical density. For crude petroleum, the SF is estimated to range from 1.08-1.32 $\mathrm{m}^3$/tonne, following a distribution $w_{\mathrm{SF}_k}^{\mathrm{crude}}$ shown in Figure E.1, which is obtained from the average daily U.S. production of crude petroleum published by the U.S. Energy Information Administration (2024) within different density categories $k$ defined by their "API gravity range", where $\sum_k w_{\mathrm{SF}_k}^{\mathrm{crude}} = 1$. Further details are provided in Appendix E. The annual trade flow of crude petroleum within API gravity range $k$ is then weighted by $w_{\mathrm{SF}_k}^{\mathrm{crude}}$:

$$T_{\mathrm{SF}_k}^{\mathrm{crude}} = T^{\mathrm{crude}} w_{\mathrm{SF}_k}^{\mathrm{crude}} \tag{22}$$

where $T^{\mathrm{crude}}$ is the total trade flow of crude petroleum obtained from the FAF5 database.

### 3.5.2 Uncertainty Evaluation for Effective Cargo Capacity

For commodities that have a range of possible SF values in the literature, $V_f^{\text{cargo, eff, av}}$ and $m_f^{\text{cargo, eff, av}}$ are by default evaluated using $\mathrm{SF}_C^{\mathrm{central}}$, which is the average of the upper $\mathrm{SF}_C^{\mathrm{upper}}$ and lower $\mathrm{SF}_C^{\mathrm{lower}}$ bounds of SF values found in the literature for commodity $C$.

$$\mathrm{SF}_C^{\mathrm{central}} = \frac{\mathrm{SF}_C^{\mathrm{lower}} + \mathrm{SF}_C^{\mathrm{upper}}}{2} \tag{23}$$

The uncertainty arising from the unknown distributions of $\mathrm{SF}_C$ within each commodity category $C$ is conservatively estimated as $\pm \frac{V_f^{\text{cargo, eff, av, upper}} - V_f^{\text{cargo, eff, av, lower}}}{V_f^{\text{cargo, eff, av, central}}}$ where $V_f^{\text{cargo, eff, av, upper}}$, $V_f^{\text{cargo, eff, av, lower}}$,

and $V_f^{\text{cargo, eff, av, central}}$ are obtained using $\text{SF}_C^{\text{upper}}$, $\text{SF}_C^{\text{lower}}$, and $\text{SF}_C^{\text{central}}$, respectively.

### 3.6 Impact of capacity and boil-off losses on cost per cargo mile

Leveraging the NavigaTE framework, the cost of cargo transport is quantified for a given vessel operating on fuel $f$ based on the average cost of owning and operating the vessel per tonne-mile of cargo transported, denoted $\left(\frac{C}{T}\right)_f$, with costs broken into capital and operating expenses:

$$\left(\frac{C}{T}\right)_f = \frac{C_f^{\text{cap}}\left(\frac{1}{\tau} + r^{\text{cap}}\right) + C_f^{\text{op, annual}}}{T_f^{\text{annual}}} \tag{24}$$

where the annual tonne-miles is given by:

$$T_f^{\text{annual}} = \sum_k V_f^{\text{cargo}} u_k s_k t^{\text{sea}} \tag{25}$$

$t^{\text{sea}}$, listed for each vessel in Table F.2, is the amount of time the vessel spends at sea over the course of one year.

The first term $C_f^{\text{cap}}\left(\frac{1}{\tau} + r^{\text{cap}}\right)$ in Equation 24 represents the annualized cost of capital, where $\tau$ is the average lifetime of the vessel − assumed to be 25 years for all vessels considered, except for the 35k DWT tanker with an assumed lifetime of 30 years. $r^{\text{cap}}$ is the average cost of capital, assumed to be 7%, and the total up-front capital expenditure $C_f^{\text{cap}}$ is given by:

$$C_f^{\text{cap}} = C^{\text{cap, vessel+power}} + \left(\frac{C}{V}\right)^{\text{cap, tank}} V_f^{\text{tank}} \tag{26}$$

where $C^{\text{cap, vessel+power}}$, with units of USD, is the combined cost of the base vessel and its power systems, comprised of propulsion, electrical, and heating. $\left(\frac{C}{V}\right)$, with units of USD/m$^3$, is the cost of the vessel's power tank, per unit of storage capacity.

The annual operating expenses $C_f^{\text{op, annual}}$ are given by:

$$C_f^{\text{op, annual}} = C^{\text{op,vessel+power}} + \left(\frac{C}{V}\right)^{\text{op, tank}} V_f^{\text{tank}} + \sum_{F\in\{o,f\}} \left(\frac{C}{m}\right)_F m_F^{\text{annual}} \tag{27}$$

where $C^{\text{op,vessel+power}}$, with units of USD/year, is the combined annual cost to operate and maintain the base vessel and its power systems. $\left(\frac{C}{V}\right)^{\text{op, tank}}$, with units of USD/m$^3$/year, is the cost to maintain the vessel's storage tanks, per unit of storage capacity. The last term $\sum_{F\in\{o,f\}}\left(\frac{C}{m}\right)_F m_F^{\text{annual}}$ quantifies the annual cost of bunkering pilot fuel oil ($F = o$) and the main alternative fuel ($F = f$) in the dual fuel vessel's tanks, where $\left(\frac{C}{m}\right)_F$, with units of USD/tonne, is the unit cost of fuel $F$ and $m_F^{\text{annual}}$ is the vessel's average annual

consumption of fuel $F$, which is related to the vessel's average power draw $P^{\text{av}}$ by:

$$m_F = \frac{\phi_F P^{\text{av}} t^{\text{sea}}}{(\text{LHV})_F \eta_f} f_F^{\text{boil-off}} \tag{28}$$

where $\phi_F$ is the fraction of annual fuel energy supplied to the dual fuel power system by either the pilot fuel oil ($F = o$) or the alternative fuel ($F = f$). For this work, the vessel is assumed to operate on its alternative fuel to the maximum extent possible, so the pilot fuel fraction is fixed to the minimum that is expected to be required when the vessels are first built − 5% for ammonia, methanol, and $LH_2$ and 1% for LNG. In the case of a conventional fuel oil vessel, no pilot fuel is needed ($\phi_o = 1$). The boil-off term $f_F^{\text{boil-off}}$, developed in Section 3.2.1, scales the amount of fuel $F$ that needs to be bunkered to compensate for BOG losses. While $f_o^{\text{boil-off}} = 1$ for the pilot fuel in a dual fuel vessel, $f_f^{\text{boil-off}}$ will in general be greater than 1 for ammonia, liquefied hydrogen, and LNG that experience boil-off.

While the first term in each of Equations 26 and 27 is in general independent of the main fuel $f$, the last terms − $\left(\frac{C}{V}\right)^{\text{cap, tank}} V_f^{\text{tank}}$ in Equation 26 and $\left(\frac{C}{V}\right)^{\text{op, tank}} V_f^{\text{tank}} + \sum_{F \in \{o,f\}} \left(\frac{C}{m}\right)_F m_F^{\text{annual}}$ in Equation 27 − will in general vary for different alternative fuel vessels.

A global average estimate of the unit cost $\left(\frac{C}{m}\right)_F$ for each fuel produced in 2024 is obtained using the fuel supply chain model presented in Eamer et al. (2025a), with hydrogen used for $LH_2$, $CH_2$ and ammonia produced via a low-temperature electrolysis pathway powered by solar − labelled "LTE (solar)" in Eamer et al. (2025a) − and carbon for methanol from direct air capture. LNG is assumed to be fossil-derived. Table F.4 summarizes these fuel cost inputs. Other cost modeling inputs can be found in the code included in the supplementary materials.

# 4 Results and Discussion

## 4.1 Tank Capacity Scaling

Figure 1 shows the design range evaluated for each vessel in the NavigaTE model using Equation 1, based on fuel and design parameters for vessels operating on conventional fuel oil. Tank capacities for dual-fuel vessels operating on alternative fuels are scaled to maintain the same design range. Bulk carriers and container ships have design ranges of approximately 30,000-45,000 nautical miles.

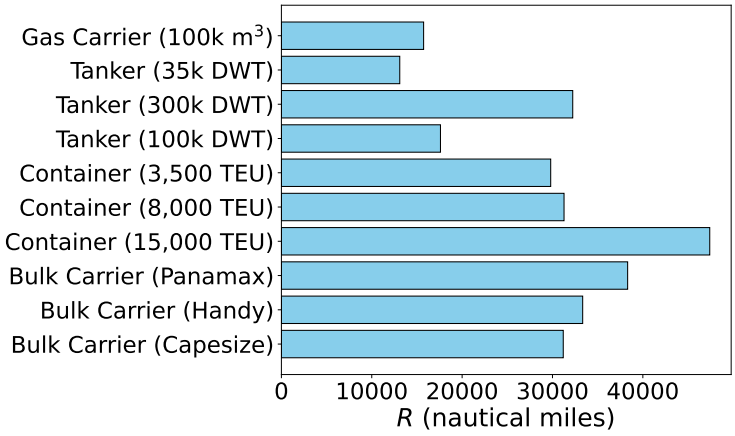


Figure 1: Design ranges for representative vessels defined in the NavigaTE model

Table 4 summarizes the effective boil-off rates for $LH_2$, LNG, and ammonia. These rates are calculated using Equation 4 and reflect the additional daily fuel consumption needed to reliquefy BOG, expressed as a percentage of total fuel volume.

| | **Fuel** | **Nominal boil-off rate $r_f^{\text{boil-off}}$ (%/day)** | **Specific Energy Consumption (kWh/kg)** | **Effective boil-off rate $r_f^{\text{boil-off, eff}}$ (%/day)** |
|---|---|---|---|---|
| Increasing boil-off rate ↓ | Ammonia | 0.03 | 0.17 | 0.0021 |
| | LNG | 0.1 | 0.59 | 0.0091 |
| | $LH_2$ | 0.5 | 5.03 | 0.16 |

Table 4: Nominal boil-off rates, specific energy consumptions, and effective boil-off rates evaluated for liquefied fuels to account for fuel loss to reliquefy the BOG.

Figure 2 presents the boil-off tank scaling factors $f_{\text{LH}_2}^{\text{boil-off}}$ for each representative vessel operating on $LH_2$, alongside the number of days $N$ required to empty each vessel's tank. The scaling factor reflects the increase in required tank volume to compensate for boil-off losses. Whiskers in the figure indicate additional scaling that would be needed if BOG were not reliquefied while at port (orange) or not used for propulsion while at sea (dark red). Boil-off factors are significantly closer to 1 for LNG and ammonia due to their lower boil-off rates.

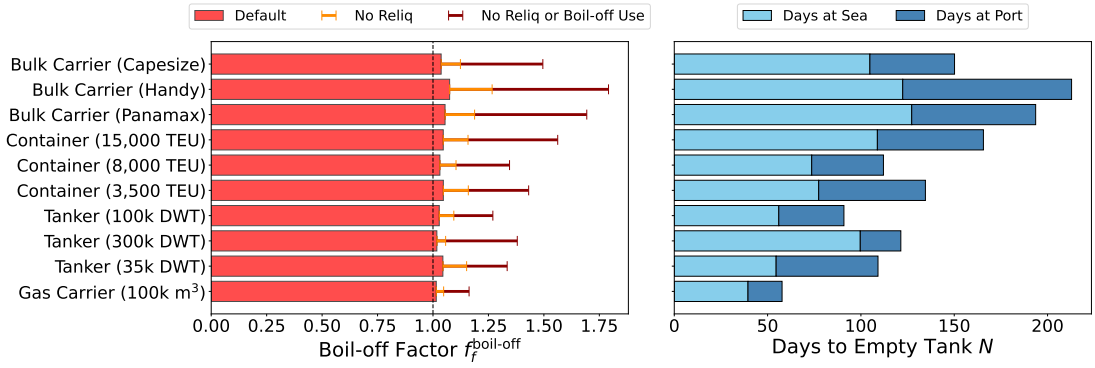


Figure 2: Left: Boil-off factors $f_{\text{LH}_2}^{\text{boil-off}}$ for liquid hydrogen across vessels. Colored whiskers indicate the additional tank scaling resulting from (orange) disabling reliquefaction while at port and (dark red) disabling both reliquefaction and the use of BOG for propulsion while at sea. Right: Time required to fully deplete each vessel's main fuel tank under typical operating conditions, expressed in days ($N$).

Figure 3 summarizes total tank scaling factors for each fuel required to maintain a fixed design range. Results are shown for both volume-based (left) and mass-based (right) scaling. The scaling factors incorporate contributions from energy density ($f^{\text{density}}$), powertrain efficiency ($f^{\text{eff}}$), and boil-off losses ($f^{\text{boil-off}}$). Whiskers indicate variation across representative vessels.

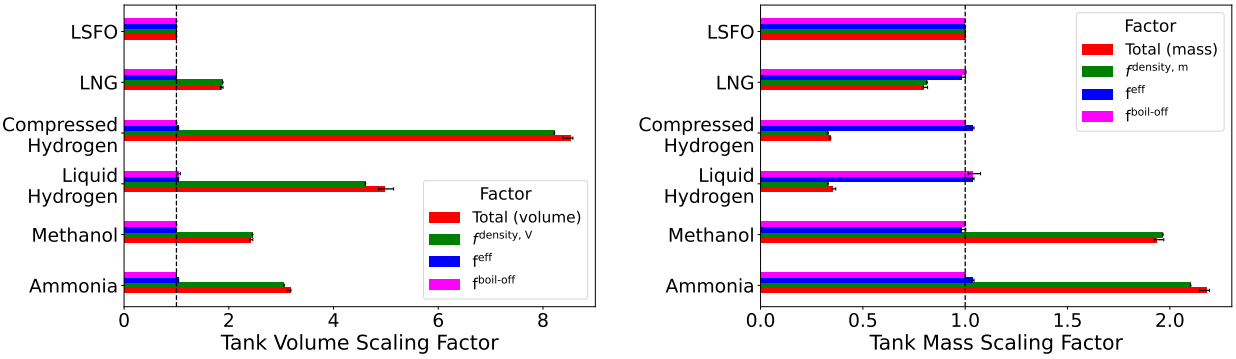


(a) Volume

(b) Mass

Figure 3: Summary of tank volume and mass scaling factors for each fuel. Whiskers show the range of values evaluated for different vessels, and bars show the average over all vessels.

The total scaling factors shown in red in Figure 3 are in line with findings in MMMCZCS (2024b) that methanol tank volumes need to scale by a factor of 2.1-2.5 to maintain a constant range for tankers, ammonia tanks by 2.9-3.1, and LNG tanks by 1.8-1.9.

**Discussion and Implications**

Maintaining conventional design ranges using alternative fuels requires substantial increases in tank volume, particularly for fuels with low volumetric energy density such as $LH_2$ and $CH_2$. Although boil-off losses increase fuel demand and tank sizing requirements, their impact remains under 10% provided that the BOG is reliquefied at port and used for propulsion at sea − without these measures, it can magnify required tank sizes by up to a factor of 1.8. These findings highlight the operational and design value of on-board reliquefaction systems and strategies to reduce port idle time.

The historically oversized design ranges of fossil-fueled vessels introduce an opportunity for alternative fuel adoption. Reducing the design range of new vessels can help reduce tank scaling requirements. However, such reductions must be carefully balanced with real-world routing needs, especially in regions where alternative refueling options are currently sparse.

This first-order analysis does not account for several important vessel design factors that may further increase tank capacity requirements for pressurized or liquefied fuels. These include the added mass and volume of insulation and structural materials required for cryogenic or high-pressure storage, the space and energy demands of auxiliary cooling systems, and the constraints imposed by non-conformal tank geometries (e.g., cylindrical or spherical tanks for pressurized or liquefied fuels). Incorporating these considerations will be an important direction for future work, as they may meaningfully alter both design feasibility and operational performance.

Further refinement of boil-off loss estimates could account for tank geometry, internal temperature gradients (Qu et al., 2019), or boil-off enhancement effects caused by sloshing in ocean waves (Smith et al., 2022). However, such refinements are of secondary concern for this work given the relatively minor contribution of boil-off losses under reasonable fuel recovery assumptions.

## 4.2 Drivers of Cargo Capacity Loss

### 4.2.1 Key Drivers

The drivers of cargo capacity loss from transitioning to alternative fuels are analyzed by examining the structure of Equations 9 and 10, which express volume- and mass-based cargo capacity loss in terms of dimensionless parameters. These equations isolate the effect of fuel properties ($\beta_f$ terms), vessel design ($\alpha$ and $f_f^{\text{pilot}}$ terms), and operational characteristics (which impact $f^{\text{boil-off}}$) on the displacement of cargo due to added tank capacity required to store alternative fuels.

To focus on vessel-level design impacts, the dimensionless scaling parameter $\beta_f$ introduced in Section

3.4.1, which reflects differences in fuel energy density and powertrain efficiency, is held fixed at its average value over all representative vessels. This parameter is largely independent of vessel geometry and is thus suitable for comparative analysis. Table 5 summarizes the average values of $\beta_f^{\text{mass}}$ and $\beta_f^{\text{volume}}$ over all representative vessels for each fuel. The variations reflect differences in effective energy efficiency $\eta_f$ between vessel types, as derived in Appendix B and summarized in Table F.3.

| **Fuel** | $\boldsymbol{\beta_f^{\text{mass}}}$ | $\boldsymbol{\beta_f^{\text{volume}}}$ |
|---|---|---|
| $CH_2$ | $\mathbf{0.342^{+0.001}_{-0.005}}$ | $\mathbf{8.76^{+0.04}_{-0.14}}$ |
| $LH_2$ | $\mathbf{0.342^{+0.001}_{-0.005}}$ | $4.78^{+0.02}_{-0.07}$ |
| Methanol | $1.93^{+0.02}_{-0.009}$ | $2.41^{+0.03}_{-0.01}$ |
| Ammonia | $\mathbf{2.18^{+0.009}_{-0.03}}$ | $3.17^{+0.01}_{-0.06}$ |
| LNG | $0.795^{+0.01}_{-0.004}$ | $\mathbf{1.84^{+0.03}_{-0.009}}$ |

Table 5: Average values of the dimensionless fuel parameters $\beta_f^{\text{mass}}$ (left) and $\beta_f^{\text{volume}}$ (right) for all fuels considered. Each value represents the average across representative vessels using the corresponding fuel. Asymmetric error bars indicate the full range of variation across vessel types. In each column, the minimum and maximum $\beta_f$ values are shown in bold to highlight alternative fuels that respectively minimize and maximize tank size scaling due to their energy density and powertrain efficiency.

#### 4.2.2 Conditions for Cargo Capacity Loss

Equations 9 and 10 imply that cargo capacity loss is strictly positive when $\beta_f > 1$ (i.e. when the alternative fuel's efficiency-corrected energy density is lower than fuel oil). Since $\beta_f^{\text{volume}} > 1$ for all alternative fuels, volumetric cargo capacity loss is expected in all cases.

In contrast, only ammonia and methanol have $\beta_f^{\text{mass}} > 1$. For hydrogen and LNG, $\beta_f^{\text{mass}} < 1$, suggesting potential gains in cargo mass capacity, unless $\beta_f^{\text{mass}} f_f^{\text{boil-off}} + f^{\text{pilot}} > 1$. In such cases, boil-off scaling factors or pilot tank requirements can offset the mass density advantage.

#### 4.2.3 Influence of Vessel Design on Cargo Capacity Loss

For a vessel operating on a given fuel, the dominant vessel design variable that affects cargo capacity loss is the tank-to-cargo capacity ratio, denoted $\alpha^{\text{mass}}$ or $\alpha^{\text{volume}}$, which depends on the baseline fuel oil vessel configuration. Equations 11 and 12 express these ratios in terms of vessel range $R$, average power $P^{\text{av}}$, average speed $s^{\text{av}}$, and cargo capacity $m_{\text{cargo}}^{\text{mass}}$ or $V_{\text{cargo}}^{\text{mass}}$. A higher $\alpha$ amplifies the absolute increase in tank capacity required when switching to a lower energy density fuel, hence resulting in a greater cargo capacity loss.

To analyze the effects of these parameters, the boil-off factor $f_f^{\text{boil-off}}$ defined in Equation 5 is expanded using a first-order Taylor approximation for $f^{\text{port}} N r_f^{\text{boil-off}} \ll 1$:

$$f_f^{\text{boil-off}} \approx 1 + \frac{1}{2} f^{\text{port}} N r_f^{\text{boil-off, eff}}$$

Substituting into Equation 9 and inserting Equation 12 yields:

$$\begin{aligned}
\text{CL}_f^{\text{volume}} &\propto \frac{P^{\text{av}} N}{V_o^{\text{cargo}}} \left[\beta_f^{\text{volume}} f_f^{\text{boiloff}} + f^{\text{pilot}} - 1\right] \\
&\approx \frac{P^{\text{av}} N}{V_o^{\text{cargo}}} \left[\beta_f^{\text{volume}} \left(1 + \frac{1}{2} f^{\text{port}} N r_f^{\text{boil-off, eff}}\right) + f^{\text{pilot}} - 1\right] \qquad (29) \\
&= \frac{P^{\text{av}} R}{V_o^{\text{cargo}} s^{\text{av}} t^{\text{day}}} \left[\beta_f^{\text{volume}} \left(1 + \frac{1}{2} f^{\text{port}} \frac{R}{s^{\text{av}} t^{\text{day}}} r_f^{\text{boil-off, eff}}\right) + f^{\text{pilot}} - 1\right] \qquad (30)
\end{aligned}$$

A similar expression for $\text{CL}_f^{\text{mass}}$ is obtained by substituting $V_o^{\text{cargo}} \to m_o^{\text{cargo}}$ and $\beta^{\text{volume}} \to \beta^{\text{mass}}$.

**Key Behavioral Insights**

- **Cargo loss scales with energy demand, or $\frac{P^{\text{av}} R}{s^{\text{av}}}$, when boil-off is negligible.** As a result, reducing either the design range or the power-to-speed ratio − for example, by minimizing time at port when the vessel continues to draw auxiliary power − can mitigate cargo loss; the latter measure provides the co-benefit of reducing overall fuel consumption.

- **Boil-off can drive superlinear scaling of cargo capacity loss with range.** When boil-off is significant, the correction factor $f_f^{\text{boil-off}}$ causes fuel requirements − and thus tank size and cargo capacity loss − to grow more than linearly with the number of days $N$ to empty the vessel's tank, and hence with the vessel's design range $R$.

- **Minimizing port time mitigates boil-off-related cargo capacity loss.** Since boil-off losses occur primarily at port (Section 3.2.1), reducing the port time fraction $f^{\text{port}}$ decreases the additional tank volume needed to offset boil-off and reliquefaction losses.

#### 4.2.4 Numerical Analysis with MC

To investigate the influence of vessel design parameters on cargo capacity loss across a broad design space, a Monte Carlo (MC) analysis is conducted using the methodology presented in Section 3.4.2. A total of 50,000 MC samples are generated by randomly varying the key design parameters listed in Table 2 across the ranges defined by NavigaTE's representative vessels. Analyzing these synthetic configurations alongside the defined vessels helps isolate general trends in cargo capacity loss from effects introduced by correlated parameter choices in real-world vessel designs, which may reflect physical or economic constraints.

Methanol serves as the initial case study due to its relatively simple behavior: it does not experience boil-off losses, and its energy density and efficiency characteristics yield both $\beta^{\text{mass}} > 1$ and $\beta^{\text{volume}} > 1$. This isolates the effect of the tank-to-cargo capacity ratio $\alpha$ on fractional cargo capacity loss. Figure 4 shows that representative vessels exhibit a strong positive correlation between the default tank volume $V_o^{\text{tank}}$ and cargo capacity $V_o^{\text{cargo}}$, while the MC samples remain uncorrelated. As a result, Figure 5 (left) shows that values of $\alpha^{\text{volume}}$ for representative vessels are tightly clustered within the range $[0.02, 0.07]$, in contrast to the much wider range $[0.001, 0.8]$ sampled in the MC dataset. These trends similarly hold for $\alpha^{\text{mass}}$.

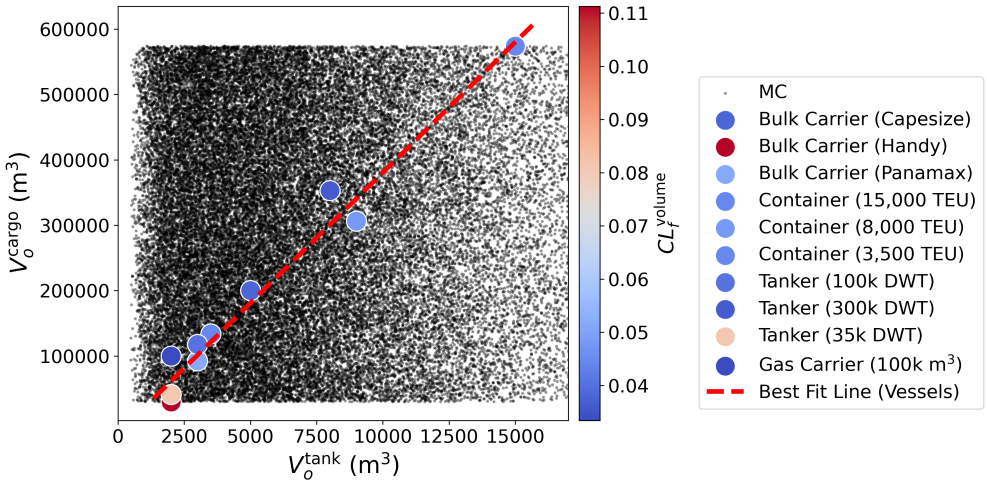


Figure 4: Scatter plot showing the relationship between cargo volume capacity $V_o^{\text{cargo}}$ and tank capacity $V_o^{\text{tank}}$ for vessels operating on methanol. MC samples are shown with small black semi-opaque markers. Representative vessels are shown with large colored markers, with the color gradient from blue (minimum) to red (maximum) defined by the fractional cargo volume loss $\text{CL}_f^{\text{volume}}$ from transitioning the vessel to methanol. A linear least squares best fit to the representative vessels is shown with a red dashed line.

Figure 5 illustrates the dominant role of the tank-to-cargo ratio $\alpha$ in driving volumetric and mass-based cargo capacity loss across fuels. For methanol (top row), variations in cargo capacity loss closely track $\alpha^{\text{volume}}$ and $\alpha^{\text{mass}}$, with small departures from linearity attributable to the pilot tank size ratio $f^{\text{pilot}}$. Ammonia exhibits similar behavior and is omitted for brevity. Cargo loss tends to be greater for smaller vessels, such as the 35k DWT Handy bulk carrier, due to their higher power-to-cargo ratios, while larger vessels like 200k DWT Capesize bulk carriers benefit from more favorable scaling, as shown for methanol in Figure 6.

For fuels subject to boil-off, such as $LH_2$ and LNG (middle and bottom rows of Figure 5), deviations from linearity arise due to the dependence of the boil-off correction factor $f_f^{\text{boil-off}}$ on the number of days $N$ required to empty the vessel's tank. As shown in Equation 5, this dependence introduces slight nonlinearity in $\text{CL}_{\text{LH2}}^{\text{volume}}$, evident in Figure 7a. Nevertheless, Figure 7b confirms that the effective boil-off rate remains low enough – even for $LH_2$ – that $f^{\text{boil-off}}$ is approximately linear in $N$ for $N < 350$, consistent with the

regime described by Equation 29.

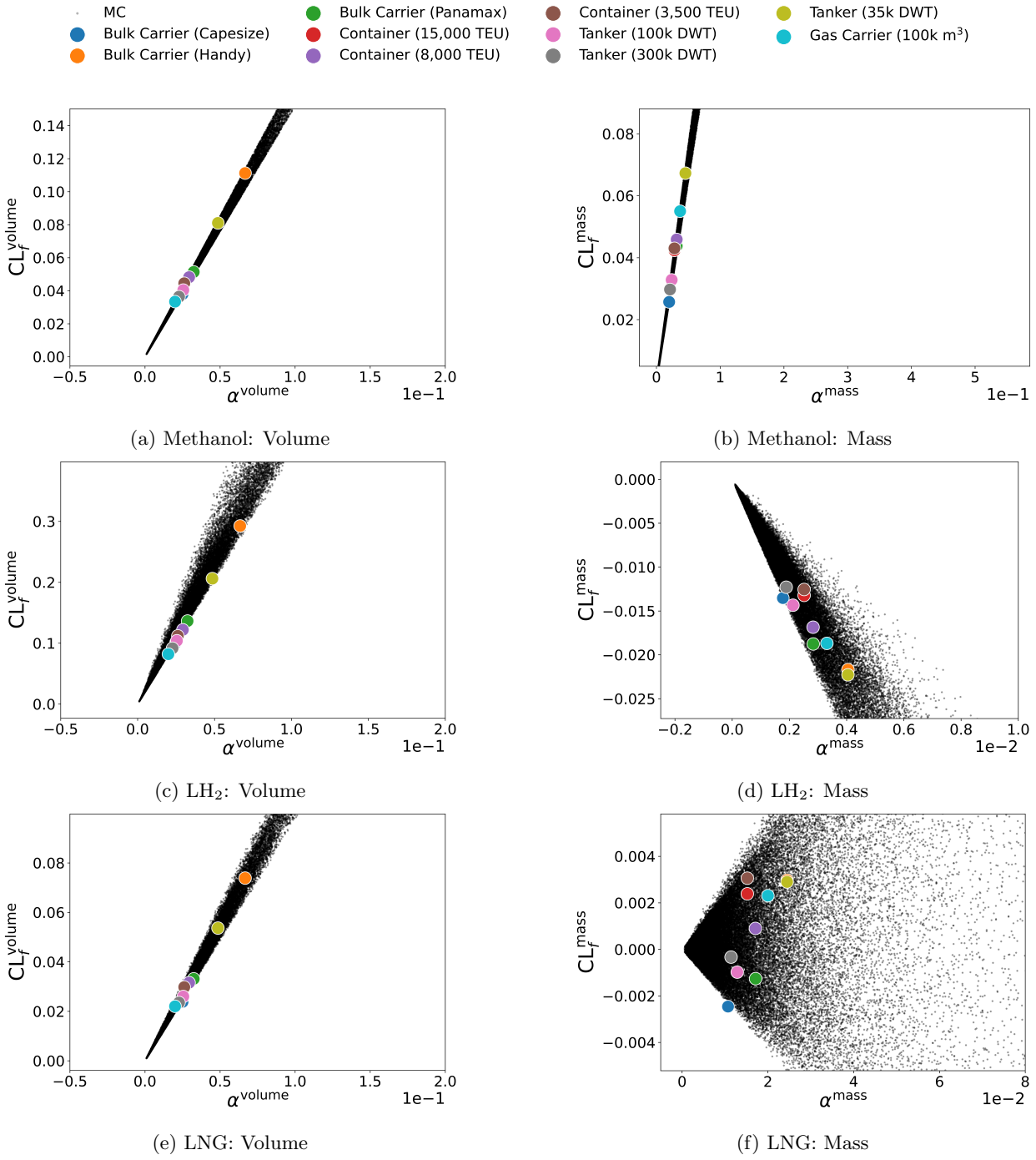


(a) Methanol: Volume

(b) Methanol: Mass

(c) $LH_2$: Volume

(d) $LH_2$: Mass

(e) LNG: Volume

(f) LNG: Mass

Figure 5: Fractional cargo volume loss $\mathrm{CL}_f^{\mathrm{volume}}$ (left) and $\mathrm{CL}_f^{\mathrm{mass}}$ (right) for vessels operating on methanol (top), $LH_2$ (middle), and LNG (bottom) as a function of the ratio $\alpha^{\mathrm{volume}}$ or $\alpha^{\mathrm{mass}}$ of tank to cargo capacity for defined vessels (large colored markers) and MC samples (small black markers).

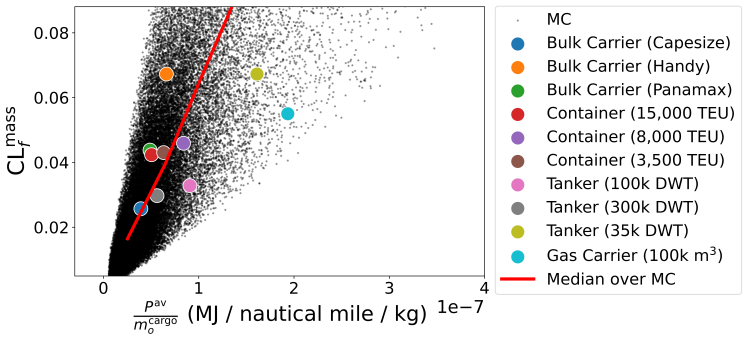


Figure 6: Fractional cargo mass loss $\mathrm{CL}_f^{\mathrm{mass}}$ as a function of the ratio $\frac{P^{\mathrm{av}}}{m_c^{\mathrm{cargo}}}$ of average power load to mass cargo capacity for defined vessels (large colored markers) and MC samples (small black markers) operating on methanol.

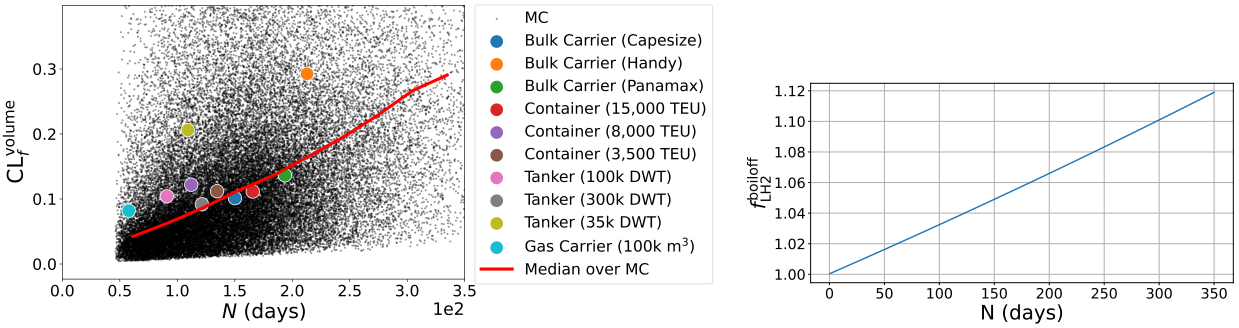


(a) $\mathrm{CL}_{\mathrm{LH2}}^{\mathrm{volume}}$ dependence

(b) $f_{\mathrm{LH2}}^{\mathrm{boiloff}}$ dependence

Figure 7: Left: Fractional cargo volume loss $\mathrm{CL}_f^{\mathrm{volume}}$ as a function of days $N$ to empty the vessel's tank, for defined vessels (large colored markers) and MC samples (small black markers) operating on $\mathrm{LH}_2$. Right: $\mathrm{LH}_2$ boil-off tank scaling factor $f_{\mathrm{LH2}}^{\text{boil-off}}$, as a function of days $N$ to empty the vessel's tank, with $f^{\mathrm{pilot}}$ and $f^{\mathrm{port}}$ fixed to typical values of 0.25 and 0.4, respectively.

While Figure 5d shows that the boil-off factor never becomes large enough to induce positive cargo mass loss for $\mathrm{LH}_2$ (since $\beta_{\mathrm{LH2}}^{\mathrm{mass}} < 1$), LNG exhibits more complex behavior, as shown in Figure 5f. Variations in the ratio of pilot to main fuel tank sizes $f^{\mathrm{pilot}}$ are sufficient to induce highly nonlinear, sign-changing behavior in both MC and representative vessels for $\mathrm{CL}_{\mathrm{LNG}}^{\mathrm{mass}}$, because $\beta_{\mathrm{LNG}}^{\mathrm{mass}} f_{\mathrm{LNG}}^{\text{boil-off}} - 1 \approx -0.2$ (Table 5). Given $f^{\mathrm{pilot}} \in [0.1, 0.286]$ (Table 6), the term $\beta_{\mathrm{LNG}}^{\mathrm{mass}} f_{\mathrm{LNG}}^{\text{boil-off}} + f^{\mathrm{pilot}} - 1$ can switch sign depending on the choice of $f^{\mathrm{pilot}}$, as illustrated in Figure 8. Intuitively, this means the combined mass of the LNG tank and pilot fuel tank in a dual-fuel vessel can exceed the mass of a conventional fuel oil tank if a relatively large pilot fuel oil tank is used.

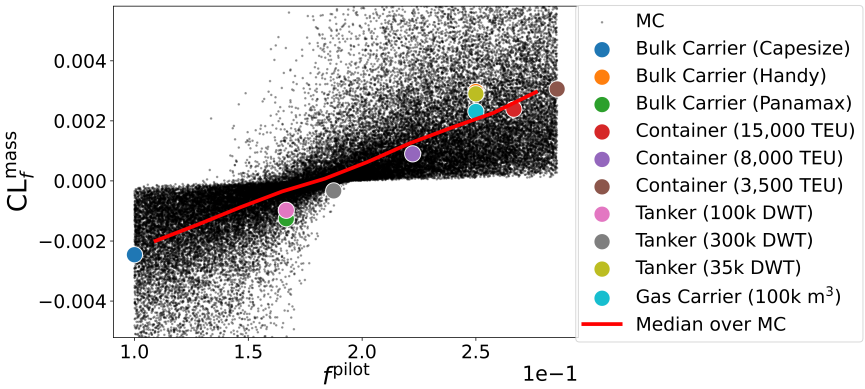


Figure 8: Fractional cargo mass loss $CL_f^{mass}$ as a function of the ratio of pilot to main fuel tank volumes $f^{pilot}$, for defined vessels (large colored markers) and MC samples (small black markers) for vessels operating on LNG.

#### 4.2.5 Discussion: Drivers of Cargo Capacity Loss

MC analysis confirms that for fuels with lower energy density than fuel oil ($\beta > 1$), cargo capacity loss is primarily driven by the nominal tank-to-cargo capacity ratio $\alpha$, with minor variation introduced by pilot tank sizing. Boil-off introduces additional spread, particularly for LNG and $LH_2$, by affecting the boil-off correction factor through changes in the number of days $N$ required to empty the vessel's tank. Representative vessels tend to cluster within narrower $\alpha$ ranges than the broader MC samples, reflecting a general design tendency to scale tank size with cargo capacity.

Based on representative vessels defined in NavigaTE, larger vessels typically exhibit lower $\alpha$ values than smaller ones. This is due in part to their lower relative power demand, and hence lower fuel consumption, for a given cargo capacity. These differences can lead to substantial disparities in cargo capacity loss. For instance, a Handy-size bulk carrier (35k DWT) may lose up to 30% of its volumetric cargo capacity to hydrogen tanks, while a Capesize bulk carrier (200k DWT) loses only 10%. For this reason, larger vessels may be better suited for early adoption of low-density alternative fuels.

While $LH_2$ tanks never displace cargo mass (since $\beta_{LH2}^{mass} << 1$), transitioning to LNG can induce either positive or negative cargo mass loss depending on the size of the pilot fuel tank. Nonlinear behavior emerges when the combined mass of the LNG and pilot fuel tanks exceeds that of the conventional fuel oil tank, particularly in small vessels or designs with large pilot tanks. For methanol, cargo mass and volume losses are generally within a similar range (3-15%), due to the comparable values of $\beta_{methanol}^{volume}$ and $\beta_{methanol}^{mass}$ (Table 5). In contrast, other alternative fuels exhibit volume losses that exceed mass losses by at least a factor of two. As a result, all else equal, methanol may be best targeted to vessels that carry volume-limited, low-density (i.e., high stowage factor) cargoes, whereas fuels with $\beta^{mass} \gg \beta^{volume}$ may be more appropriate for high-density

(low stowage factor) cargoes. These stowage factor effects are detailed in Section 4.3.

Across both analytical and simulation approaches, the dominant drivers of cargo capacity loss are the tank-to-cargo ratio $\alpha$ and the fuel's effective energy density relative to fuel oil $\beta$. Smaller vessels with higher $\alpha$ values are especially susceptible to large losses. Operational parameters, such as design range, average speed, and port time, can further modulate these outcomes, particularly under boil-off conditions.

## 4.3 Effective Cargo Capacity Loss as a Function of Stowage Factor

Table 6 summarizes the nominal mass and volume capacities for each representative vessel defined in NavigaTE. As only one capacity measure − either mass or volume − is specified by default, the alternate capacity measure is estimated using the methodology in Section 3.4.3. These capacities are used to evaluate effective cargo capacity and cargo capacity loss as a function of stowage factor (SF), following Equations 16 through 18.

| **Vessel Class** | **Size Label** | **Nominal Mass Capacity (tonnes)** | **Nominal Volume Capacity ($m^3$)** | **Default Nominal Capacity Measure** |
|---|---|---|---|---|
| Bulk Carrier | Capesize | 200k | 200k | Mass |
| | Pamanax | 75k | 92.5k | |
| | Handy | 35k | 30k | |
| Tanker | 300k DWT | 300k | 353k | Mass |
| | 100k DWT | 100k | 118k | |
| | 35k DWT | 35k | 41.2k | |
| Container Ship | 15,000 TEU | 423k | 574k | Volume |
| | 8,000 TEU | 225k | 306k | |
| | 3,500 TEU | 98.6k | 134k | |
| Gas carrier | 100k DWT | 42.8k | 100k | Volume |

Table 6: Summary of nominal mass and volume cargo capacity estimates for each representative vessel. The default measure of nominal capacity − mass or volume − defined in the NavigaTE model is indicated in the last column for each vessel class.

Figure 9 illustrates how effective mass and volume cargo capacities change as a function of SF for a sample bulk carrier (left) and container ship (right). Solid and dashed lines respectively indicate volume- and mass-limited regimes.

For low-SF cargoes (i.e. dense materials such as iron ore), the cargo capacity is mass-limited. In this regime, the effective mass capacity remains constant, and the effective volume capacity increases linearly

with SF, from Equations 16 and 17:

$$m_{f,\mathrm{SF}}^{\mathrm{cargo,\ eff}} = m_o^{\mathrm{cargo}}(1 - \mathrm{CL}_f^{\mathrm{mass}}), \quad V_{f,\mathrm{SF}}^{\mathrm{cargo,\ eff}} = \mathrm{SF} \cdot m_{f,\mathrm{SF}}^{\mathrm{cargo,\ eff}}$$

As SF increases, the vessel transitions to a volume-limited regime, where the effective volume capacity remains fixed and effective mass capacity decreases inversely with SF.

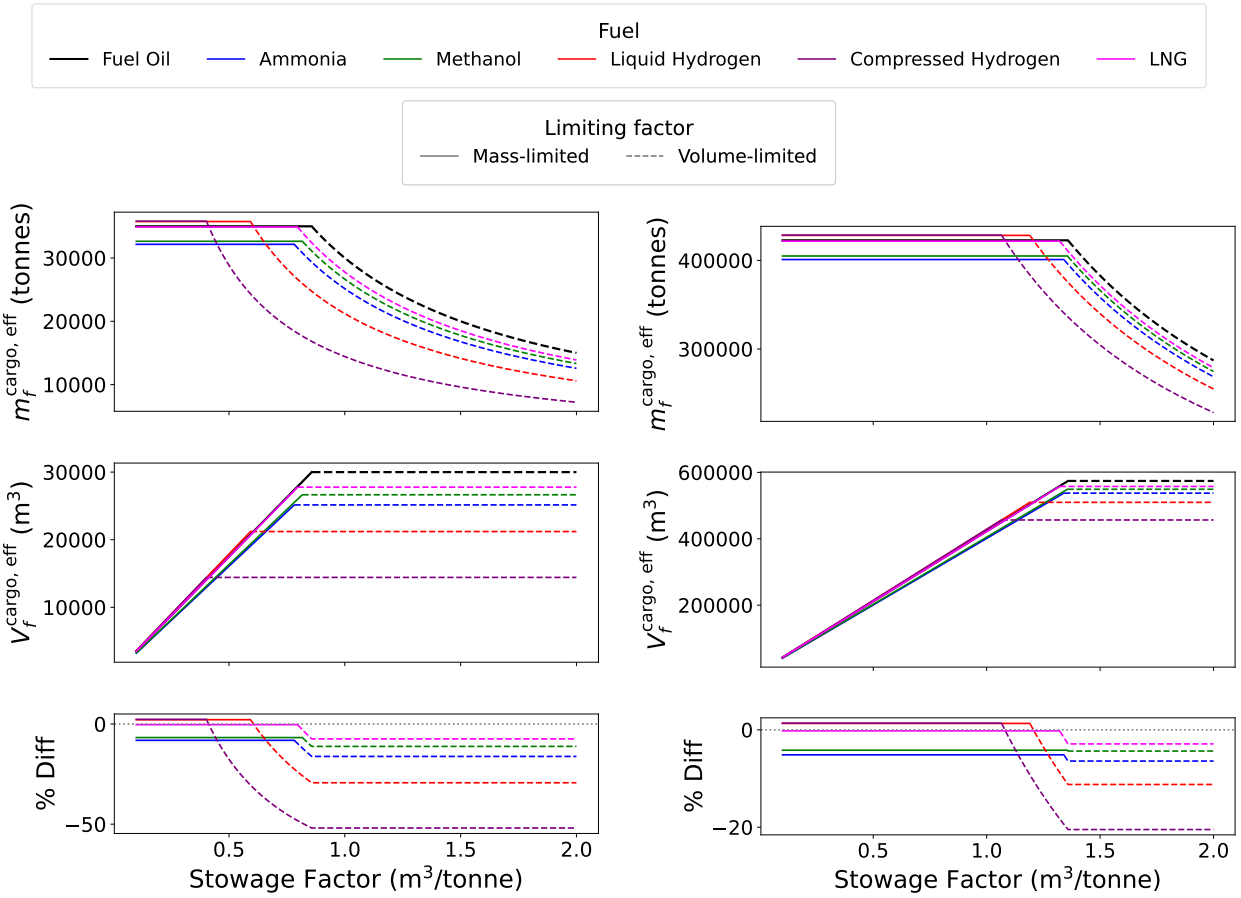


(a) Handy Bulk Carrier

(b) 15,000 TEU Container

Figure 9: Comparison of effective mass (top panel) and volume (center panel) cargo capacity for each fuel as a function of the vessel's cargo SF, for a sample bulk carrier and container ship. The bottom panel shows the percent difference in cargo capacity for the vessel operating on each fuel relative to fuel oil.

### 4.3.1 Trends Across Fuels and Vessel Types

As shown in the bottom panels of Figure 9, the relative reduction in cargo capacity for alternative fuels compared to conventional fuel oil is in general larger when the vessels are volume-limited, as $\beta_f^{\mathrm{volume}} > \beta_f^{\mathrm{mass}}$. This effect is most pronounced for $CH_2$ and $LH_2$, for which effective capacities are slightly larger than fuel oil in the mass-limited regime and can be reduced by over 50% in the volume-limited regime, and least

pronounced for methanol, whose effective capacity loss relative to fuel oil increases by only a few percent between mass-limited and volume-limited regimes.

While LNG experiences a larger jump in cargo loss in transitioning from mass-limited to volume-limited regimes compared with methanol and ammonia, its overall cargo loss remains smaller than methanol and ammonia (under 10%) in both regimes. In the mass-limited regime, $CH_2$ and LNG can slightly outperform conventional fuel oil. Their higher LHV allows them to meet vessel energy demands with smaller tank masses, thereby preserving or even increasing effective cargo mass capacity.

#### 4.3.2 Application to study cargo capacity loss for vessels carrying U.S. Imports and Exports

Using the methods described in Section 3.5.1, average effective cargo capacities are evaluated for each representative vessel transporting projected 2025 U.S. import and export flows, as tabulated in the FAF5 dataset. Figure 10 compares the effective cargo capacities of vessels operating on alternative fuels (hatched bars) with those using conventional fuel oil (solid bars) across the four vessel classes considered in this study.

Across vessel classes, most U.S. import and export cargoes are found to result in volume-limited capacities, leading to substantial reductions in effective cargo capacity relative to nominal. Vessels operating on LNG (magenta bars in Figure 10) exhibit the smallest reductions in capacity, attributable to LNG's relatively high LHV and moderate mass density. In contrast, $CH_2$ (purple bars) results in the most severe capacity penalties due to its very low mass density. The following sections examine these outcomes by vessel class, contextualized by the associated stowage factor distributions and evaluation methods for average cargo capacity loss.

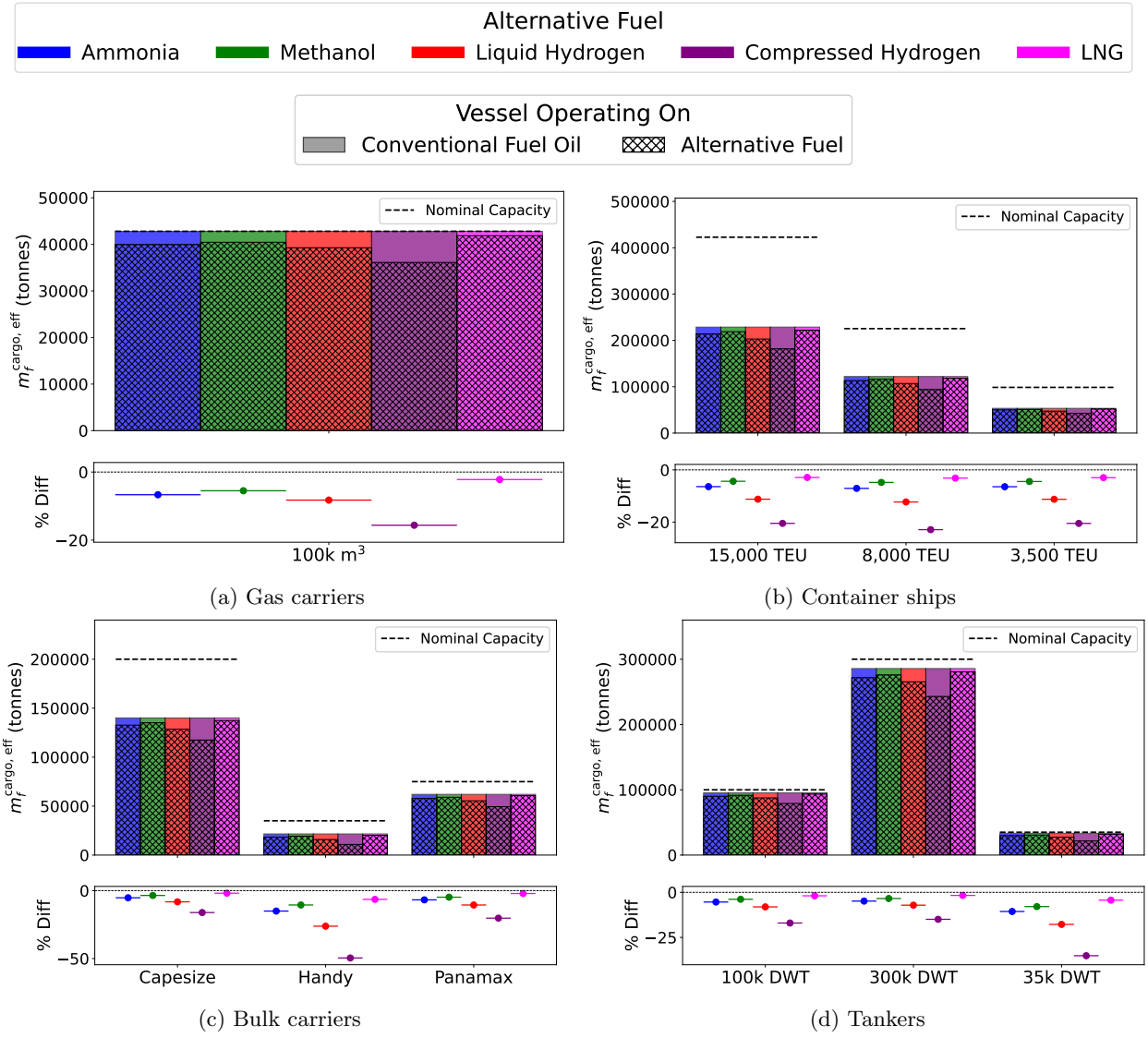


(a) Gas carriers

(b) Container ships

(c) Bulk carriers

(d) Tankers

Figure 10: Effective mass cargo capacity $m_f^{\text{cargo, eff}}$ of representative vessels, evaluated using central cargo SFs ($\text{SF}^{\text{central}}$) of U.S. import and export flows. Hatched bars in the top panel show the effective capacity of vessels operating on alternative fuels, and solid bars show the effective capacity on fuel oil for comparison. The lower panel shows the percent difference in effective cargo capacity with the alternative fuel relative to fuel oil. The nominal cargo mass capacity of each vessel is shown with a black dashed horizontal line for comparison.

### Gas carriers

For gas carriers, a single cargo stowage factor (SF) of 2.34 m$^3$/tonne is assumed, based on the density of LNG. With this SF, capacities are consistently volume-limited. Consequently, the largest cargo capacity losses relative to conventional fuel oil are observed for hydrogen fuels, consistent with the trends in Figure 9. Cargo capacity losses range from 2% for LNG to 16% for $CH_2$. Because the mass capacity is derived from the volume capacity using the same SF, the effective cargo capacity of vessels operating on fuel oil remains

equal to the nominal capacity, despite being volume-limited.

**Container ships**

As described in Section 3.5.1, container ship capacities are evaluated using a single tonne-mile-weighted average stowage factor, $\mathrm{SF}^{\mathrm{av}}$, computed via Equation 21 over all commodities assumed to be transported by container ships. Figure 11 presents the weighted distribution of stowage factors based on the lower ($\mathrm{SF}_C^{\mathrm{lower}}$), upper ($\mathrm{SF}_C^{\mathrm{upper}}$), and central ($\mathrm{SF}_C^{\mathrm{central}}$) values for each commodity $C$. This analysis yields an average stowage factor of $\mathrm{SF}^{\mathrm{av}} = 2.51 \pm 0.78$ for container ships.

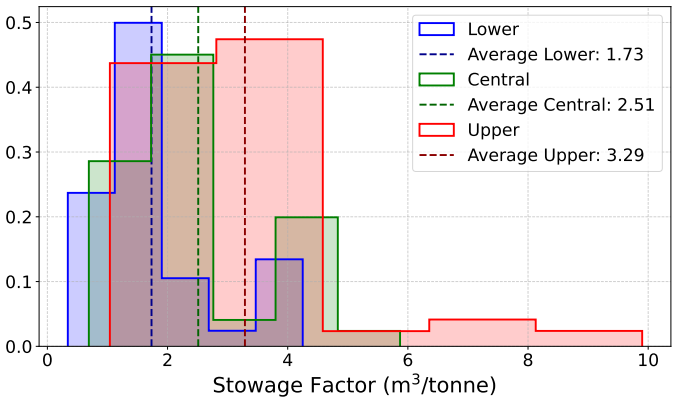


Figure 11: Upper, lower, and central SF distributions of cargo carried by container ships.

Similar to gas carriers, this $\mathrm{SF}^{\mathrm{av}}$ results in volume-limited cargo capacities for all container vessels, whether operating on fuel oil or alternative fuels. Accordingly, the largest capacity penalties occur for hydrogen fuels, with losses ranging from 3% for LNG to 24% for $CH_2$. For container ships, these losses are relatively consistent across vessel sizes. Unlike gas carriers, the effective capacity of container vessels running on conventional fuel oil is substantially (46%) lower than the nominal capacity. This discrepancy arises because the nominal mass capacity, based on the maximum container weight of 28,180 kg (see Section 3.4.3), implies a minimum cargo SF of only 1.4 $\mathrm{m}^3$/tonne, which is well below the average value of 2.51 observed for U.S. imports and exports.

**Bulk carriers and tankers**

Because bulk carriers and tankers typically transport a single commodity per voyage, their average effective cargo capacity is evaluated as a tonne-mile-weighted average of capacities calculated individually for each commodity, as described in Section 3.5.1.

Figure 12 shows the tonne-mile-weighted distributions of evaluated cargo capacities for a representative bulk carrier operating on fuel oil (left) and $LH_2$ (right), using central SF values for each commodity. Dashed vertical lines indicate the tonne-mile-weighted averages across all commodities. Cargoes with low stowage factors, such as metallic ores, tend to be mass-limited (colored red), while the majority are volume-limited

(colored blue). When comparing vessels operating on $LH_2$ (Figure 12b) with those using fuel oil (Figures 12a), the same commodities increasingly fall into the volume-limited regime when using lower-density fuels due to the additional volume occupied by the fuel tanks.

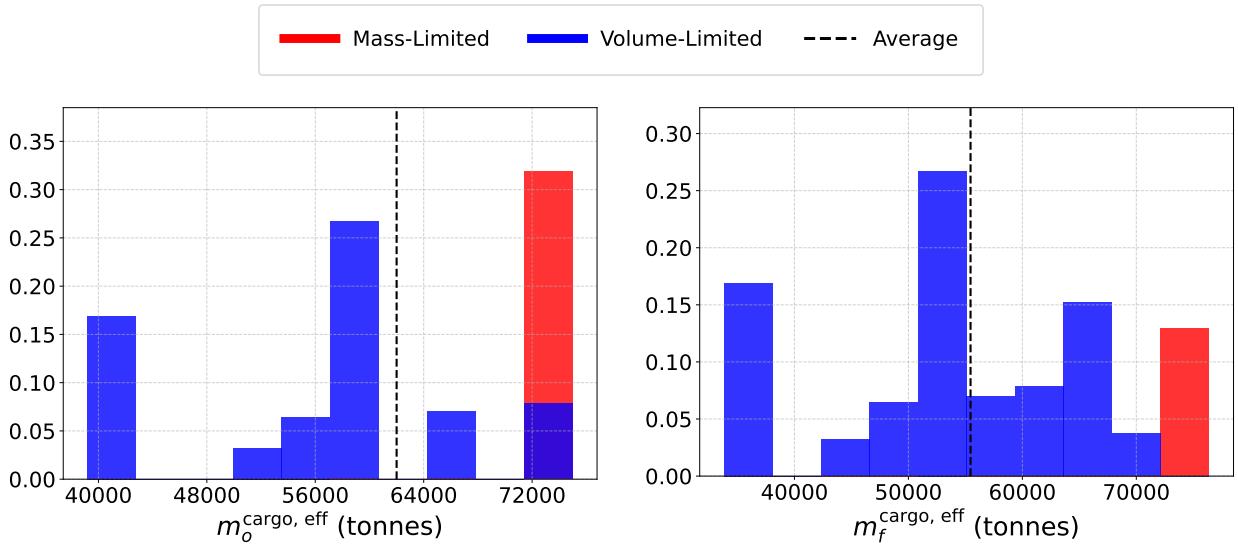


(a) Panamax (Fuel Oil)

(b) Panamax ($LH_2$)

Figure 12: Tonne-mile weighted distributions of cargo mass capacity for a sample bulk carrier operating either on fuel oil or $LH_2$, using central SF values. Black dashed vertical lines show the tonne-mile weighted average.

Because most cargoes are volume-limited, the average mass capacity of bulk carriers and tankers operating on fuel oil is generally lower than the nominal capacity. However, this difference is less pronounced (5–38%) compared to container ships (46%), reflecting smaller differences between $SF^{av}$ and the stowage factor associated with the nominal volume capacity.

### 4.3.3 Impact of Stowage Factor Uncertainty

Figure 13 compares cargo capacity impacts evaluated with $SF^{lower}$ (Figure 13a) and $SF^{upper}$ (Figure 13b) for each commodity to assess the impact of uncertainty in the tonne-mile distribution within the commodity's SF range, as described in Section 3.5.2. The resulting uncertainties in effective cargo capacity are assessed at 10–30% for bulk carriers, 23–45% for container ships, and 0.7% for tankers. However, because both alternative fuel and fuel oil vessels are affected similarly by changes in SF assumptions, the resulting uncertainty in relative cargo capacity loss CL remains under 15% across all fuels and representative vessels.

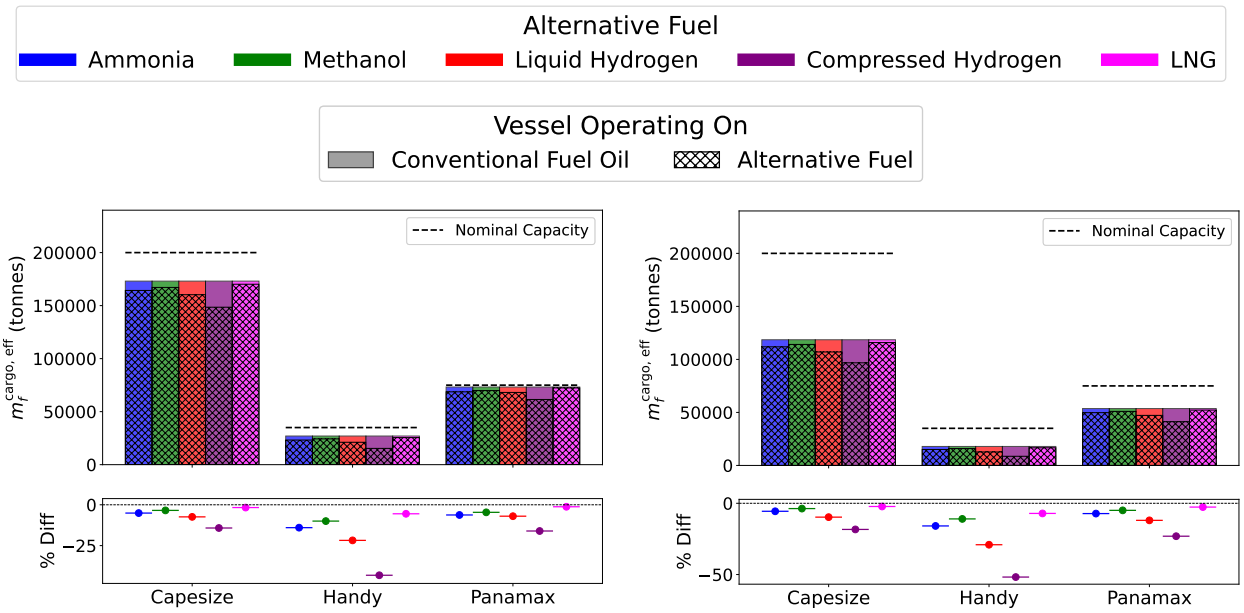


(a) Lower SF bound ($SF^{lower}$)

(b) Upper SF bound ($SF^{upper}$)

Figure 13: Comparison of nominal and effective vessel capacities for bulk carriers using either the lower or upper bound of SF factor estimates.

### 4.3.4 Discussion and Implications

The results in this section highlight the importance of accounting for cargo stowage factor in determining the effective cargo capacity, and the significance of cargo losses from switching to alternative fuels.

For mass-limited voyages carrying dense (low-SF) cargo, reductions in effective cargo capacity with alternative fuels are modest – up to 10% for ammonia and methanol, near zero for LNG, and negative for hydrogen. As cargo becomes less dense, vessels transition to a volume-limited regime, in which switching to fuels with low volumetric energy density – particularly $CH_2$ or $LH_2$ – can induce cargo losses over 50%. Among the alternatives, LNG exhibits the lowest overall capacity penalties thanks to its favorable mass and energy density. Methanol also performs relatively well, with losses remaining under 10% overall and the smallest difference between mass- and volume-limited regimes, making it less sensitive to changes in cargo density. Effective cargo capacity losses for vessels operating on ammonia can be up to 8% by mass and up to 16% by volume.

Importantly, SF-driven limitations are not unique to alternative fuels. Conventional fuel oil vessels also experience reduced effective capacity when carrying low-density cargo. For example, container ships using fuel oil show a 46% reduction in cargo capacity relative to nominal design, solely due to cargo SF.

In the U.S. trade application, payloads are predominantly volume-limited for all vessel classes, and consistently so for container ships and gas carriers, making the latter classes particularly sensitive cargo loss

from switching to fuels with low volumetric density.

These findings highlight the importance of accounting for anticipated cargo stowage factors in fuel transition analyses. Because the effect of fuel choice on cargo capacity varies with stowage factor, neglecting this parameter can lead to significant misrepresentation of cargo capacity trade-offs.

## 4.4 Impact on cost of cargo transport

To evaluate the economic consequences of reduced cargo capacity, the cost of transport per tonne-mile was calculated using the methodology in Section 3.6. Figure 14 compares the impact of cargo capacity loss and boil-off on transport costs for selected fuels. Results are shown for hydrogen fuels − representing the most significant capacity penalties − and LNG, which incurs the smallest.

The figure indicates that cargo capacity loss dominates increased transport costs, with added fuel costs due to reliquefaction of BOG adding only a modest additional burden − up to 5% for $LH_2$. Accounting for these effects substantially increases the cargo transport cost premiums for $CH_2$ and $LH_2$ relative to fuel oil. On average, the most substantial cost increases occur for container ships and bulk carriers, and the smallest for gas carriers.

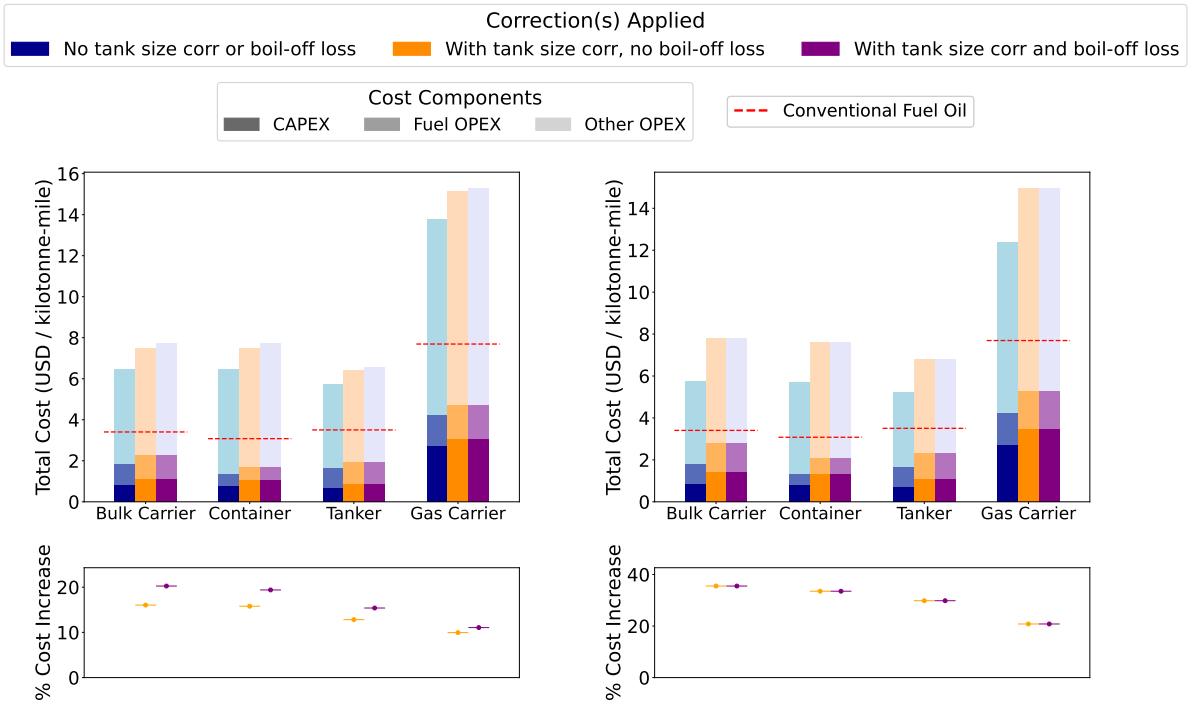


(a) $LH_2$

(b) $CH_2$

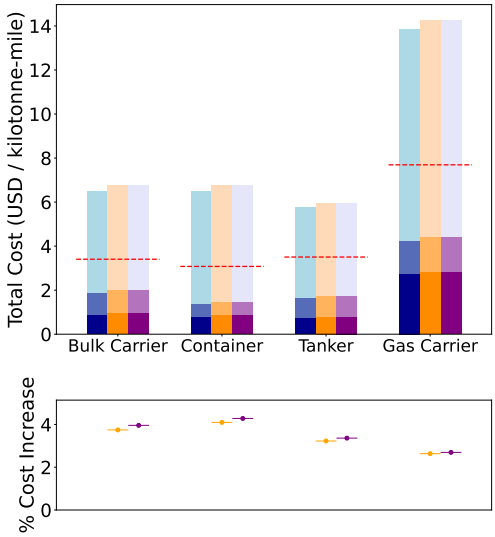


(c) LNG

Figure 14: Total cost per tonne-mile of cargo transport for representative vessel classes operating on alternative fuels. For each vessel class, results are averaged across all vessel sizes. Within each vessel class, adjacent bars from left to right show the successive application of the tank size correction (orange), followed by additional fuel costs due to BOG reliquefaction (purple). For comparison, the total cost for vessels operating on fuel oil is indicated by red horizontal dashed lines. The lower panel shows the percent cost increase resulting from successive application of each correction.

Table 7 presents cost increases for each vessel size and fuel, accounting for cargo loss and added fuel costs to reliquify BOG. Among the fuels evaluated, $CH_2$ yields the highest cost penalties (21–112%), followed by

$LH_2$ (11–46%), ammonia (6–20%), methanol (4–12%), and LNG (3–8%).

| | | Increase in Cost / tonne-mile | | | | |
|---|---|---|---|---|---|---|
| **Vessel Class** | **Size Label** | **LNG** | **Methanol** | **Ammonia** | **Liquid $H_2$** | **Compr. $H_2$** |
| Bulk Carrier | Capesize | 3% | 4% | 7% | 15% | 26% |
| | Pamanax | 4% | 5% | 9% | 20% | 34% |
| | Handy | 8% | 12% | 20% | 46% | 112% |
| Tanker | 300k DWT | 4% | 4% | 6% | 12% | 24% |
| | 100k DWT | 3% | 4% | 7% | 13% | 25% |
| | 35k DWT | 6% | 9% | 13% | 27% | 60% |
| Container Ship | 15,000 TEU | 4% | 5% | 9% | 20% | 34% |
| | 8,000 TEU | 4% | 5% | 9% | 19% | 37% |
| | 3,500 TEU | 4% | 5% | 8% | 19% | 32% |
| Gas carrier | 100k $m^3$ | 3% | 6% | 8% | 11% | 21% |
| | | Increasing cost penalty ⟶ | | | | |

Table 7: Cost penalty, expressed as percentage increase in cost per tonne mile, for each vessel class and size due to tank size corrections and fuel loss to boil-off reliquefaction. Fuels are listed from left to right in order of increasing cost penalty.

**Discussion and Implications**

Reductions in cargo capacity are found to dominate cost increases from switching to alternative fuels over fuel loss to BOG reliquefaction. The volumetric inefficiency of $CH_2$ in particular imposes prohibitive cost penalties, especially for smaller vessels for which tank-to-cargo ratios are highest. Ammonia, methanol and LNG offer more modest cargo capacity losses and better preservation of transport economics.

The findings highlight an important shift in comparative fuel economics. Fuels that appear affordable when assessed on a per-MJ or per-kg basis may prove significantly more expensive once vessel-level capacity constraints are considered. Accordingly, techno-economic and lifecycle analyses that neglect cargo displacement risk underestimating real-world operational costs.

These insights have clear implications for policy and investment. Incentives, subsidies, and infrastructure planning must account not only for fuel production costs and emissions profiles but also for the physical consequences of fuel switching on vessel capacity. Failure to do so may distort comparative assessments and lead to suboptimal decarbonization strategies. Incorporating cargo-related effects into fuel evaluation frameworks is essential to ensure economically and operationally feasible fleet transitions.

# 5 Conclusions

This study quantifies the impact of alternative marine fuels on vessel cargo capacity and transport costs, focusing on the interplay between fuel properties, vessel design, and cargo characteristics. The primary driver of cargo loss is the tank-to-cargo capacity ratio ($\alpha^{\text{mass}}$ or $\alpha^{\text{volume}}$) of the baseline fuel oil vessel. Smaller vessels, with higher $\alpha$, experience disproportionately greater losses, highlighting a structural advantage for large vessels in fuel transitions.

Additional penalties arise from pilot tank requirements and boil-off gas (BOG) losses. While the boil-off tank scaling factor $f^{\text{boil-off}}$ increases nonlinearly with fuel residence time, its impact remains modest − typically under 10% − when boil-off gas is used for propulsion and excess is reliquefied at port. Without these measures, required tank volume can increase by up to 80%, emphasizing the importance of on-board BOG recovery systems and minimizing idle time.

Effective cargo capacity depends on whether the vessel is mass- or volume-limited, a condition determined by the stowage factor (SF) of the cargo. Most U.S. cargo flows are volume-limited, making low-volumetric-density fuels like compressed and liquid hydrogen especially costly in terms of displaced cargo. Even vessels using conventional fuel oil show significant effective capacity loss when transporting low-density cargo, underscoring that SF affects all fuels.

Monte Carlo simulations confirm that cargo loss scales nearly linearly with $\alpha$ for fuels like ammonia and methanol, while boil-off introduces additional variation for LNG and liquid hydrogen. Among all fuels, LNG incurs the smallest cargo penalties due to its favorable energy density, while compressed hydrogen suffers the greatest.

Boil-off-related fuel costs are minor, but cargo displacement substantially increases the cost per tonne-mile − by over 100% in some small vessels using compressed hydrogen. The results carry important implications for fleet transition planning. Transition strategies should prioritize larger, more power-efficient vessels on routes with frequent bunkering opportunities that can enable short design ranges, for which cargo losses can be significantly reduced. Fleet transition models should account for cargo displacement and anticipated cargo stowage factors to ensure accurate assessments of fuel viability.

# Glossary

## Symbols

| Symbol | Units | Description |
|---|---|---|
| $f$ | None | Used as a subscript to denote any fuel choice. |
| $o$ | None | Used as a subscript to specifically denote conventional fuel oil. |
| $(\text{LHV})_f$ | MJ/kg | Lower heating value of fuel $f$. |
| $\eta_f$ | None | Average conversion efficiency of usable energy for fuel $f$ into energy output by the vessel's propulsion, heat, and electrical power systems. |
| $\rho_f$ | $\text{kg/m}^3$ | Mass density of fuel $f$. |
| $r_f^{\text{boil-off}}$ | $\text{days}^{-1}$ | Fractional loss of fuel $f$ per day from the vessel's main fuel tank due to boil-off. |

Table 8: Fuel-specific parameters used in the study

| Symbol | Units | Description |
|---|---|---|
| R | nautical miles | Vessel design range, defined as the average distance the vessel can travel at sea on a single fuel tank. |
| $N$ | days | Average number of days the vessel can travel at sea on a single fuel tank. |
| $P_{\text{av}}$ | MW | Average power used by the main engine over all operating conditions |
| $\left(\frac{P}{s}\right)^{\text{av}}$ | MJ / nautical mile | Average ratio of engine power to vessel speed. Can also be thought of as the average energy consumed by the engine per unit distance traveled by the vessel. |
| $V_f^{\text{cargo}}$ | $\text{m}^3$ | Cargo volume capacity. |
| $m_f^{\text{cargo}}$ | kg | Cargo mass capacity, defined as the maximum mass of cargo that can be loaded onto the vessel. |
| $V_f^{\text{tank}}$ | $\text{m}^3$ | Tank volume capacity with fuel $f$, defined as the maximum volume of fuel that can be contained in the main tank of a vessel design to run primarily on fuel $f$. |
| $m_f^{\text{tank}}$ | kg | Tank mass capacity with fuel $f$, definedi as the maximum mass of fuel $f$ that can be contained in the main tank of a vessel design to run primarily on fuel $f$. |
| $V^p$ | $\text{m}^3$ | Volume capacity of the pilot fuel tank in a dual fuel vessel. |
| $n^p$ | $\text{m}^3$ | Mass capacity of the pilot fuel tank in a dual fuel vessel. |
| $P^e$ | MW | Average power demand of the vessel's electrical system while at sea. |
| $P^h$ | MW | Average power demand of the vessel's heat system while at sea. |
| $s$ | knots | Vessel speed. |
| $u$ | None | Fractional cargo capacity utilization of the vessel, where u=1 is fully loaded and u=0 is fully unloaded. |
| $f_k$ | None | Fraction of time spent by the vessel in condition k, defined by speed $s_k$ and cargo capacity utilization $u_k$. |
| $P^p_{s,u}$ | MW | Speed-utilization-power surface for the vessel's propulsion system, defined as the propulsion system load needed for the vessel to travel at speed $s$ with cargo capacity utilization $u$. |

Table 9: Vessel design parameters considered in the study

| Symbol | Definition or Reference Equation | Description |
|---|---|---|
| $f_f^{\text{density, m}}$ | $\frac{(\text{LHV})_o}{(\text{LHV})_f}$ | Multiplicative factor that scales the mass capacity $m_o$ of a conventional fuel oil tank such that it can contain an equivalent amount of usable energy for fuel $f$. |
| $f_f^{\text{density, V}}$ | $\frac{(\text{LHV})_o \rho_o}{(\text{LHV})_f \rho_f}$ | Multiplicative factor that scales the volume capacity $m_o$ of a conventional fuel oil tank such that it can contain an equivalent amount of usable energy when operating with an alternative fuel $f$. |
| $f_f^{\text{eff}}$ | $\frac{\eta_o}{\eta_f}$ | Multiplicative factor that scales the capacity $C_o$ of a conventional fuel oil tank to account for the different average energy conversion efficiency of the vessel running on another fuel $f$. |
| $f_f^{\text{boil-off}}$ | $\frac{\eta_o}{\eta_f}$ | Multiplicative factor that scales the capacity $C_o$ of a conventional fuel oil tank to compensate for fuel loss to boil-off when transitioning to a liquefied alternative fuel $f$. |
| $f^{\text{tank, pilot}}$ | $\frac{V^{\text{tank, pilot}}}{V_o^{\text{tank}}}$ | Ratio of pilot fuel oil tank capacity $V^{\text{tank, pilot}}$ in a dual fuel vessel to nominal main fuel tank capacity $V_o^{\text{tank}}$ when running on conventional fuel oil. |
| $\alpha^m$ | $\frac{m_o^{\text{tank}}}{m_o^{\text{cargo}}}$ | Ratio of the main tank's mass capacity to the vessel's cargo mass capacity when running on conventional fuel oil $o$. |
| $\alpha_V$ | $\frac{V_o^{\text{tank}}}{V_o^{\text{cargo}}}$ | Ratio of the main tank's volume capacity to the vessel's cargo volume capacity when running on conventional fuel oil $o$. |
| $\beta^m$ | $f_f^{\text{density,m}} f_f^{\text{eff}}$ | Combined multiplicative factor that scales the mass of a conventional fuel oil tank such that the vessel's energy conversion systems can output an equivalent amount of energy when operating with an alternative fuel $f$. |
| $\beta^V$ | $f_f^{\text{density,V}} f_f^{\text{eff}}$ | Combined multiplicative factor that scales the volume of a conventional fuel oil tank such that the vessel's energy conversion systems can output an equivalent amount of energy when operating with an alternative fuel $f$. |
| $\text{CL}_f^{\text{V}}$ | $\frac{V_o^{\text{cargo}} - V_f^{\text{cargo}}}{V_o^{\text{cargo}}}$ | Relative loss in cargo volume capacity for a vessel operating with alternative fuel $f$, relative to the cargo capacity $V_o^{\text{cargo}}$ of the vessel operating with conventional fuel oil. |
| $\text{CL}_f^{\text{m}}$ | $\frac{m_o^{\text{cargo}} - m_f^{\text{cargo}}}{m_o^{\text{cargo}}}$ | Relative loss in cargo mass capacity for a vessel operating with alternative fuel $f$, relative to the cargo capacity $m_o^{\text{cargo}}$ of the vessel operating with conventional fuel oil. |

Table 10: Dimensionless terms obtained from parameters listed in Tables 8 and 9

| Symbol | Units | Description |
|---|---|---|
| $\rho_{\text{cargo}}$ | tonnes / $m^3$ | Average density of cargo carried by a vessel. |
| SF | $m^3$/tonne | Stowage factor, defined as the inverse of the average cargo density. |
| $m_{\text{eff}}$ | tonnes | Effective cargo mass capacity of a vessel, accounting for the average stowage factor of its cargo. |
| $V_{\text{eff}}$ | $m^3$ | Effective cargo volume capacity of a vessel, accounting for the average stowage factor of its cargo. |
| $\eta_f$ | None | Average conversion efficiency of usable energy for fuel $f$ into energy output by the vessel's propulsion, heat, and electrical power systems. |
| $\rho_f$ | kg/$m^3$ | Mass density of fuel $f$. |
| $r_f$ | $\text{days}^{-1}$ | Fractional loss of fuel $f$ per day from the vessel's main fuel tank due to boil-off. |

Table 11: Parameters used to evaluate a vessel's effective cargo capacity, accounting for cargo stowage factor as presented in Section 3.5.

| Symbol | Units | Description |
|---|---|---|
| $\left(\frac{C}{T}\right)_f$ | USD/tonne-mile | Average total cost per unit of transport work for vessel running on fuel $f$. |
| $C_f^{\text{cap}}$ | USD | Capital expenditure of a vessel running on fuel $f$, including vessel and power system cost and tank cost. |
| $\tau$ | years | Vessel lifetime. |
| $r^{\text{cap}}$ | None | Annualized cost of capital. |
| $C_f^{\text{op, annual}}$ | USD/year | Annual operating cost of vessel running on fuel $f$. |
| $T_f^{\text{annual}}$ | tonne-miles/year | Annual cargo miles transported by the vessel. |
| $t^{\text{sea}}$ | days | Amount of time the vessel spends at sea per year. |
| $C^{\text{cap, vessel+power}}$ | USD | Combined capital cost of base vessel and its power systems. |
| $\left(\frac{C}{V}\right)^{\text{cap, tank}}$ | USD/$m^3$ | Capital cost per unit tank volume. |
| $V_f^{\text{tank}}$ | $m^3$ | Volume capacity of tank required for fuel $f$. |
| $C^{\text{op, vessel+power}}$ | USD/year | Annual operating and maintenance cost of base vessel and power systems. |
| $\left(\frac{C}{V}\right)^{\text{op, tank}}$ | USD/$m^3$/year | Annual operating cost per unit tank volume. |
| $\left(\frac{C}{m}\right)_F$ | USD/kg | Unit cost of fuel $F$ (either $f$ or $o$). |
| $m_F^{\text{annual}}$ | kg/year | Annual fuel consumption of fuel $F$ (either $f$ or $o$). |
| $\phi_F$ | None | Fraction of total annual fuel energy supplied by fuel $F$. |

Table 12: Parameters used to evaluate the total cost per unit of cargo transport for a given vessel in Section 3.6.

## Abbreviations

| Abbreviation | Definition |
|---|---|
| *Fuel and Energy Terms* | |
| LHV | Lower Heating Value (MJ/kg), the usable energy released during combustion, excluding latent heat of vaporization. |
| SF | Stowage Factor ($m^3$/tonne), the inverse of cargo density, representing volume per unit mass of cargo. |
| LNG | Liquefied Natural Gas, primarily methane cooled to cryogenic liquid form. |
| $LH_2$ | Liquefied Hydrogen, cryogenically cooled for liquid storage. |
| $CH_2$ | Hydrogen compressed to 700 bar for storage. |
| BOG | Boil-off gas from cryogenic fuel storage. |
| *Operational Metrics* | |
| nm | Nautical mile, equivalent to 1.852 kilometers. |
| MW | Megawatt, unit of power equal to $10^6$ watts. |
| TEU | Twenty-foot Equivalent Unit, standardized volumetric measure for containerized cargo. |
| DWT | Deadweight Tonnage, total weight a vessel can safely carry including cargo, fuel, and supplies. |
| *Modeling and Cost Terms* | |
| MC | Monte Carlo, a simulation method using random sampling to analyze uncertainty. |
| *Model and Data References* | |
| MMMCZCS | Mærsk Mc-Kinney Møller Center for Zero Carbon Shipping. |
| NavigaTE | Model developed by MMMCZCS to simulate the operation and evolution of the global fleet with the uptake of alternative fuels and technologies. |
| FAF5 | Freight Analysis Framework version 5, a dataset from the U.S. Department of Transportation that tabulates domestic, import, and export freight flows for the U.S. |
| GREET | Greenhouse gases, Regulated Emissions, and Energy use in Technologies, a lifecycle model developed by Argonne National Laboratory. |

Table 13: Abbreviations used in the paper.


# Acknowledgements

This work was carried out with support from the Future Energy Systems Center through the MIT Energy Initiative. The NavigaTE model used in the study was developed at the Mærsk Mc-Kinney Møller Center for Zero Carbon Shipping. The authors thank Frederik Lehn for support with NavigaTE implementation, Prof. Christopher Douglas for early conceptual contributions and insights, and Randall Field for feedback and expertise that helped refine this work.

## Funding

This work was supported by the Future Energy Systems Center through the MIT Energy Initiative.

## CRediT authorship contribution statement

**Danika Eamer:** Conceptualization, Methodology, Software, Investigation, Writing - Original draft, Visualization **Stamatis Stamatelopoulos:** Validation, Methodology, Writing – review & editing **Amr Elbanhawy:** Methodology **Fotini Christia:** Project administration **Themistoklis Sapsis:** Project administration, Supervision, Methodology, Writing – review & editing **Elsa Olivetti:** Project administration, Supervision, Funding acquisition, Writing – review & editing

## Declaration of competing interest

The authors declare that they have no known competing financial interests or personal relationships that could have appeared to influence the work reported in this paper.

## Declaration of Generative AI and AI-assisted technologies in the writing process

During the preparation of this work, the authors used ChatGPT to assist with language editing, clarity, and formatting of tables. After using this tool, the authors reviewed and edited the content as needed and take full responsibility for the content of the published article.

## Data availability

All data inputs used for this work are available in this GitHub repository (Eamer et al., 2025b).

## Supplementary materials

All inputs and code used for this work are available in this GitHub repository (Eamer et al., 2025b).

# A Derivation of Vessel Design Range

A vessel's design range $R_f$ with fuel $f$ is related to the ratio of the net mass $m_f^{\text{tank, net}}$ of fuel available in the fuel tank and the average rate $\left(\frac{dm_{\text{fuel}}}{dr}\right)$ at which fuel is consumed by the vessel's main propulsion, electricity, and heat systems with respect to the distance $r$ traveled by the vessel.

$$R_f = \frac{m_f^{\text{tank, no boil-off}}}{\left(\frac{dm^{\text{fuel}}}{dr}\right)^{\text{av}}} = \frac{m_f^{\text{tank}}}{f_f^{\text{boil-off}}\left(\frac{dm^{\text{fuel}}}{dr}\right)^{\text{av}}} \tag{A.1}$$

where the boil-off scaling factor $f_f^{\text{boil-off}} \geq 1$ amplifies the tank size to correct for the loss of fuel to boil-off gasification for fuels that are compressed or cooled for storage in liquid form (details in Section 3.2.1). The average fuel consumption rate over the full period to empty the tank $\left(\frac{dm^{\text{fuel}}}{dr}\right)^{\text{av}}$ can be expressed in terms of the vessel's average speed $s^{\text{av}}$ and power consumption $P^{\text{av}}$ over that period:

$$\begin{aligned}
\left(\frac{dm^{\text{fuel}}}{dr}\right)^{\text{av}} &= \frac{\left(\frac{dm^{\text{fuel}}}{dt}\right)^{\text{av}}}{\left(\frac{dr}{dt}\right)^{\text{av}}} \\
&= \frac{1}{(\text{LHV})_f}\frac{\left(\frac{dE^{\text{fuel}}}{dt}\right)^{\text{av}}}{s^{\text{av}}} \\
&= \frac{1}{(\text{LHV})_f \eta_f}\frac{\left(\frac{dE}{dt}\right)^{\text{av}}}{s^{\text{av}}} \\
&= \frac{1}{(\text{LHV})_f \eta_f}\frac{P^{\text{av}}}{s^{\text{av}}}
\end{aligned} \tag{A.2}$$

The vessels's average power draw is given by:

$$\begin{aligned}
P^{\text{av}} &= P^{\text{sea, av}} f^{\text{sea}} + P^{\text{port, av}}(1 - f^{\text{sea}}) \\
&= (P^{\text{prop, av}} + P^{\text{elec, sea}} + P^{\text{heat, sea}}) f^{\text{sea}} \\
&\quad + (P^{\text{elec, port}} + P^{\text{heat, port}})(1 - f^{\text{sea}})
\end{aligned} \tag{A.3}$$

where $P^{\text{sea, av}}$ is the vessel's average power load while underway (referred to as "at sea") and $P^{\text{port, av}}$ is the average load when the vessel is stopped (referred to as "at port").

While the vessels's average electrical and heating loads - $P^{\text{elec, sea}}$ and$P^{\text{heat, sea}}$ and at port - $P^{\text{elec, port}}$ and$P^{\text{heat, port}}$ - are assumed independent of voyage conditions, its propulsion load $P^{\text{prop}}$ is assumed to vary with its speed $s$ and fractional cargo capacity utilization $u$, which can range from 0 (fully unloaded) to 1

(loaded to full draft), and thus is in general expressed as the speed - utilization - power surface $P_{s,u}^{\text{prop, sea}}$. Approximating the vessel's sailing conditions by a discrete distribution of speeds and cargo capacity utilizations $\{(s_k, u_k, f_k)\}$, where $f_k$ denotes the time spent in condition $k$ and $\sum_k f_k = 1$:

$$P^{\text{prop, av}} = \sum_k P_{s_k,u_k} f_k \tag{A.4}$$

and the average speed over all time spent at sea and at port is given by:

$$s^{\text{av}} = f^{\text{sea}} \sum_k s_k f_k \tag{A.5}$$

Inserting Equation A.2 into A.1 yields:

$$R = \frac{(\text{LHV})_f \eta_f m_f^{\text{tank}} s^{\text{av}}}{f_f^{\text{boil-off}} P^{\text{av}}} = \frac{(\text{LHV})_f \eta_f \rho_f V_f^{\text{tank}} s^{\text{av}}}{f_f^{\text{boil-off}} P^{\text{av}}} \tag{A.6}$$

where $\rho_f = \frac{m_f^{\text{tank}}}{V_f^{\text{tank}}}$ is the mass density of the fuel stored in the tank.

Table A.1 shows a sample speed-utilization-power surface defined in NavigaTE for a Capesize bulk carrier, and Table A.2 shows a sample speed-power curve defined for a 15,000 twenty-foot equivalent (TEU) container vessel. Table A.3 shows a sample $\{(s_k, u_k, f_k)\}$ distribution defined in NavigaTE for the Capesize bulk carrier. All surfaces, curves, and $\{(s_k, u_k, f_k)\}$ can be found in the code included in the supplementary material.

| **Speed s (knots)** | **Propulsion Power $\mathbf{P^{prop}}_{s,u=0}$ at $u = 0$ (MW)** | **Propulsion Power $\mathbf{P^{prop}}_{s,u=1}$ at $u = 1$ (MW)** |
|---|---|---|
| 8.0 | 2.56 | 3.20 |
| 9.0 | 3.43 | 4.29 |
| 10.0 | 4.48 | 5.60 |
| 11.0 | 5.70 | 7.13 |
| 12.0 | 7.12 | 8.90 |
| 13.0 | 8.76 | 10.95 |
| 14.0 | 10.79 | 13.48 |
| 14.5 | 12.01 | 15.01 |

Table A.1: Discrete speed-utilization-power surface $P_{s,u}^{\text{prop}}$ defined in the NavigaTE model for the Capesize bulk carrier vessel. Source: NavigaTE version 2 defaults time stamped on June 18, 2025 (Eamer et al., 2025b).

| **Speed s (knots)** | **Propulsion Power $\mathbf{P^{prop}}_s$ (MW)** |
|---|---|
| 12 | 9.6 |
| 13 | 12.1 |
| 14 | 14.7 |
| 15 | 16.4 |
| 16 | 19.6 |
| 17 | 23.1 |
| 18 | 27.2 |
| 19 | 31.9 |
| 20 | 37.4 |
| 21 | 43.4 |
| 22 | 50.4 |
| 23 | 58.4 |

Table A.2: Discrete speed-power curve $P_s^{\text{prop}}$ defined in the NavigaTE model for the 15,000 twenty-foot equivalent container vessel. Source: NavigaTE version 2 defaults time stamped on June 18, 2025 (Eamer et al., 2025b).

| $k$ | $\mathbf{s_k}$ **(knots)** | $\mathbf{u_k}$ | $\mathbf{f_k}$ |
|---|---|---|---|
| 0 | 11.2 | 1.0 | 0.5 |
| 1 | 13.6 | 0.0 | 0.5 |

Table A.3: Discrete speed and capacity utilization distribution $\{(s_k, u_k, f_k)\}$ defined for the Capesize bulk carrier. Source: NavigaTE version 2 defaults time stamped on June 18, 2025 (Eamer et al., 2025b).

# B Derivation of Combined Energy Efficiency

A vessel is assumed to draw fuel from onboard tank(s) to supply energy to its propulsion (prop), electricity (elec), and heat systems. In a given vessel operating condition $k$ and mode (either at sea or at port), the total rate of fuel energy consumption $P_k^{\text{fuel}}$ can be written as:

$$P_k^{\text{fuel, mode}} = \begin{cases} \dfrac{P^{\text{prop}}_{s_k,u_k}}{\eta^{\text{prop}}} + \dfrac{P^{\text{elec, sea}}}{\eta^{\text{elec}}} + \dfrac{P^{\text{heat, sea}}}{\eta^{\text{heat}}}, & \text{if mode} = \text{sea} \\ \dfrac{P^{\text{elec, port}}}{\eta^{\text{elec}}} + \dfrac{P^{\text{heat, port}}}{\eta^{\text{heat}}}, & \text{if mode} = \text{port} \end{cases} \tag{B.1}$$

where $P^{\text{sys, mode}}$ and $\eta^{\text{sys}}$ denote the power demand and energy conversion efficiency, respectively, for the vessel operating in the given mode. For a given mode, $P^{\text{elec, mode}}$ and $P^{\text{heat, mode}}$ are assumed to be approximately independent of the vessel's operating condition in the given mode.

As discussed in Appendix A, $P_{s,u}^{\text{prop}}$ is assumed to vary while the vessel is at sea according to its speed $s$

and fractional cargo capacity utilization $u$. Approximating the vessel's operating conditions with the discrete distribution $\{(s_k, u_k, f_k)\}$, the vessel's average combined power system load $P^{\text{av}}$ over all operating conditions is given by Equation A.3 in Appendix A.

The total energy drawn from the fuel tanks, accounting for system-level efficiencies, is:

$$\begin{aligned} P_f^{\text{fuel, av}} &= \sum_{\text{mode}\in\{\text{sea, port}\}} \left( \sum_k P_k^{\text{fuel}} f_k \right) f^{\text{mode}} \\ &= \left( \frac{P^{\text{prop, av}}}{\eta_f^{\text{prop}}} + \frac{P^{\text{elec, sea}}}{\eta_f^{\text{elec}}} + \frac{P^{\text{heat, sea}}}{\eta_f^{\text{heat}}} \right) f^{\text{sea}} \\ &\quad + \left( \frac{P^{\text{elec, port}}}{\eta_f^{\text{elec}}} + \frac{P^{\text{heat, port}}}{\eta_f^{\text{heat}}} \right) (1 - f^{\text{sea}}) \end{aligned} \tag{B.2}$$

where $P^{\text{prop, av}} = \sum_k P_{s_k,u_k}^{\text{prop}} f_k$. The vessel's combined energy conversion efficiency over its operating profile is then defined as the ratio of total useful output to total fuel input:

$$\eta_f = \frac{P^{\text{av}}}{P_f^{\text{fuel, av}}} = \frac{(P^{\text{prop, av}} + P^{\text{elec, sea}} + P^{\text{heat, sea}}) f^{\text{sea}} + (P^{\text{elec, port}} + P^{\text{heat, port}})(1 - f^{\text{sea}})}{\left( \frac{P^{\text{prop, av}}}{\eta_f^{\text{prop}}} + \frac{P^{\text{elec}}}{\eta_f^{\text{elec}}} + \frac{P^{\text{heat}}}{\eta_f^{\text{heat}}} \right) f^{\text{sea}} + \left( \frac{P^{\text{elec}}}{\eta_f^{\text{elec}}} + \frac{P^{\text{heat}}}{\eta_f^{\text{heat}}} \right) (1 - f^{\text{sea}})} \tag{B.3}$$

For a given fuel, an average combined energy conversion efficiency can be evaluated over the ten vessel classes listed in Table 6:

$$\eta_f^{\text{av}} = \frac{\sum_k \eta_{f,k}}{N^{\text{vessels}}} \tag{B.4}$$

where $k$ iterates over each of the ten vessel classes $N^{\text{vessels}} = 10$ is the total number of vessels.

Values of $\eta_f^{\text{av}}$ are tabulated for each fuel, along with the maximum and minimum value over all vessels, in Table F.3.

# C Derivation of Boil-off Factor

For a liquefied fuel $f$, the boil-off factor magnifies the tank's mass capacity from $m_f^{\text{tank, no boil-off}}$ to $m_f^{\text{tank}}$ such that additional fuel can be bunkered to ensure that an effective mass $m_f^{\text{tank, no boil-off}}$ of fuel is available to the vessel's power systems after accounting for fuel loss due to boil-off and reliquefaction while the vessel is stopped over the $N$ days that the vessel takes to empty its tank.

**General $f_d$**

Lacking detailed knowledge of when a given vessel will be at port vs. at sea as it empties its fuel tank, let $f_d$ represent an arbitrary discrete probability that the vessel is at port on day $d$ over the course of its voyage. If $f^{\text{sea}}$ is the average fraction of time the vessel spends at sea over the course of the year, $f_d$ must on average satisfy:

$$\sum_{d=1}^{N} \frac{f_d}{N} \equiv f^{\text{port}} = 1 - f^{\text{sea}} \tag{C.1}$$

In the absence of any other fuel draw, the fuel $F_d^{\text{no draw}}$ remaining in the tank after $d$ days would be:

$$F_d^{\text{no draw}} = m_f^{\text{tank}} \prod_{i=1}^{d} (1 - r_f^{\text{boil-off, eff}})^{f_i} \tag{C.2}$$

where $r_f^{\text{boil-off, eff}}$ is the effective rate of loss of fuel $f$ to boil-off while the vessel is at port, due to additional fuel used to power the boil-off gas reliquefaction process.

However, the vessel's power systems also draw fuel from the tank at an average daily rate of $\frac{m_{f,\text{ no boil-off}}}{N}$, which is accounted for with the following correction:

$$F_d^{\text{with draw}} = m_f^{\text{tank}} \prod_{i=1}^{d} (1 - r_f^{\text{boil-off, eff}})^{f_i} - \frac{m_f^{\text{tank, no boil-off}}}{N} \sum_{k=0}^{d-1} (1 - r_f)^{f_k} \tag{C.3}$$

Applying the requirement that the tank fully empty after N days at sea (i.e. $F_N^{\text{with draw}} = 0$), the boil-off factor $f^{\text{boil-off}} = \frac{m_f^{\text{tank}}}{m_f^{\text{tank, no boil-off}}}$ is evaluated as follows:

$$\begin{aligned} 0 &= m_f^{\text{tank}} \prod_{i=1}^{d} (1 - r_f^{\text{boil-off, eff}})^{f_i} - \frac{m_f^{\text{tank, no boil-off}}}{N} \sum_{k=0}^{d-1} (1 - r_f)^{f_k} \\ f_f^{\text{boil-off}} &= \frac{m_f^{\text{tank}}}{m_f^{\text{tank, no boil-off}}} = \frac{1}{N} \frac{\sum_{k=0}^{N-1} (1 - r_f)^{f_k}}{\prod_{i=1}^{d} (1 - r_f^{\text{boil-off, eff}})^{f_i}} \end{aligned} \tag{C.4}$$

**Special case: $f_d = f^{\text{port}}$**

The closed-form expression for $f_f^{\text{boil-off}}$ used in this work is obtained under a simplifying assumption that, on average, the daily probability of a vessel being at port follows a uniform distribution $f_d = f^{\text{port}} = 1 - f^{\text{sea}}$. With this assumption, Equation C.2 simplifies to:

$$F_d^{\text{no draw, special}} = m_f^{\text{tank}} (1 - r_f^{\text{boil-off, eff}})^{f^{\text{port}} d} \tag{C.5}$$

For any $q \neq 1$, the geometric sum $\sum_{k=0}^{d-1} q^k$ evaluates to $\frac{1-q^d}{1-q}$. Letting $q = (1 - r_f^{\text{boil-off, eff}})^{f^{\text{port}}}$, Equation C.3 simplifies to:

$$F_d^{\text{with draw}} = m_f^{\text{tank}}(1 - r_f^{\text{boil-off, eff}})^{f^{\text{port}}d} - \frac{m_f^{\text{tank, no boil-off}}}{N} \frac{1 - (1 - r_f^{\text{boil-off, eff}})^{f^{\text{port}}d}}{1 - (1 - r_f^{\text{boil-off, eff}})^{f^{\text{port}}}} \tag{C.6}$$

In this case, the boil-off factor simplifies to:

$$f_f^{\text{boil-off}} = \frac{1}{N} \frac{1}{(1 - r_f^{\text{boil-off, eff}})^{f^{\text{port}}N}} \frac{1 - (1 - r_f^{\text{boil-off, eff}})^{f^{\text{port}}N}}{1 - (1 - r_f^{\text{boil-off, eff}})^{f^{\text{port}}}} \tag{C.7}$$

# D Supplementary Tables and Figures for Stowage Factor Analysis

| **Field** | **Description** |
|---|---|
| Mode | Transportation mode used to carry the shipment. Entries used for this work are filtered to exclude all modes except water. |
| Trade Type | Type of trade (domestic, foreign import, or foreign export). Entries used for this work are filtered to only include foreign import and foreign export. |
| Commodity | Commodity being carried by the shipment (43 distinct commodities tabulated). Commodities are filtered for one at a time. |
| Ton-miles | Total ton-miles of commodities shipped (unit: Million ton-miles). For each commodity, ton-miles are summed over all filtered rows to obtain the total ton-miles of the given commodity carried into or out of US ports by water to/from foreign destinations/origins. |

Table D.1: Information fields in the Freight Analysis Framework (FAF5) (Federal Highway Administration, 2025) data used for this work.

| Commodity | Lower SF ($m^3$/tonne) | Lower SF source | Upper SF ($m^3$/tonne) | Upper SF source |
|---|---|---|---|---|
| Cereal grains | 1.3 | Cargo Handbook (Cereals) (BMT, 2025) | 1.8 | Cargo Handbook (Cereals) (BMT, 2025) |
| Animal feed | 1.23 | Cargo Handbook (Soybeans) (BMT, 2025) | 2.07 | Cargo Handbook (Fishmeal) (BMT, 2025) |
| Other ag prods. | 1.17 | Cargo Handbook (Sugar) (BMT, 2025) | 3.55 | Cargo Handbook (Peanuts) (BMT, 2025) |
| Building stone | 0.67 | Cargo Handbook (Limestone) (BMT, 2025) | 0.84 | Cargo Handbook (Limestone) (BMT, 2025) |
| Natural sands | 1.3 | Handy Bulk (Sand) (HandyBulk LLC, 2025) | 1.5 | Handy Bulk (Sand) (HandyBulk LLC, 2025) |
| Gravel | 1.4 | Handy Bulk (Gravel) (HandyBulk LLC, 2025) | 1.7 | Handy Bulk (Gravel) (HandyBulk LLC, 2025) |
| Nonmetallic minerals | 0.67 | Cargo Handbook (Limestone) (BMT, 2025) | 1.15 | Cargo Handbook (Clays) (BMT, 2025) |
| Metallic ores | 0.29 | Cargo Handbook (Ores) (BMT, 2025) | 0.8 | Cargo Handbook (Ores) (BMT, 2025) |
| Coal | 1.1 | Cargo Handbook (Coal and Coke) (BMT, 2025) | 1.3 | Cargo Handbook (Coal and Coke) (BMT, 2025) |
| Fertilizers | 1.0 | Handy Bulk (Fertilizer) (HandyBulk LLC, 2025) | 1.3 | Handy Bulk (Fertilizer) (HandyBulk LLC, 2025) |
| Logs | 0.99 | Handy Bulk (Logs) (HandyBulk LLC, 2025) | 2.55 | Handy Bulk (Logs) (HandyBulk LLC, 2025) |
| Wood prods. | 1.2 | Handy Bulk (Pellets) (HandyBulk LLC, 2025) | 3.5 | Handy Bulk (Wood Chips) (HandyBulk LLC, 2025) |
| Nonmetal min. prods. | 0.61 | Cargo Handbook (Cement) (BMT, 2025) | 1.98 | Cargo Handbook (Glass Sheets) (BMT, 2025) |
| Base metals | 0.24 | Cargo Handbook (Lead Ore) (BMT, 2025) | 1.11 | Cargo Handbook (Zinc) (BMT, 2025) |

Table D.2: Stowage factor (SF) range estimates and sources for commodities assumed to be carried by bulk carriers.

Table D.3: Stowage factor (SF) range estimates and sources for commodities assumed to be carried by container ships.

| **Commodity** | **Lower SF ($m^3$/tonne)** | **Lower SF source** | **Upper SF ($m^3$/tonne)** | **Upper SF source** |
|---|---|---|---|---|
| Meat/seafood | 2.26 | Cargo Handbook (Frozen Meat) (BMT, 2025) | 3.96 | Cargo Handbook (Frozen meat) (BMT, 2025) |
| Milled grain prods. | 1.34 | Cargo Handbook (Rice) (BMT, 2025) | 1.67 | Handy Bulk (Wheat) (HandyBulk LLC, 2025) |
| Other foodstuffs | 1.17 | Cargo Handbook (Sugar) (BMT, 2025) | 3.96 | Cargo Handbook (Frozen meat) (BMT, 2025) |
| Alcoholic beverages | 1.7 | Freight Charter (Beer Cartons) (Freight Chartering Operations, 2015) | 1.87 | Freight Charter (Beer Cases) (Freight Chartering Operations, 2015) |
| Tobacco prods. | 3.12 | Freight Charter (Tobacco Cases) (Freight Chartering Operations, 2015) | 3.96 | Freight Charter (Tobacco Cases) (Freight Chartering Operations, 2015) |
| Pharmaceuticals | 2.0 | BPS Bulk Density Guide (Pharmaceutical Mix) (Best Product Solutions, Inc., 2025) | 7.1 | BPS Bulk Density Guide (Pharmaceutical Lubricant) (Best Product Solutions, Inc., 2025) |
| Plastics/rubber | 0.56 | JingDong Rubber Co., LTD (JingDong Rubber Co., LTD, 2025) | 1.15 | Grigorescu et al. 2019 (Grigorescu et al., 2019) (Table 4, PP) |
| Newsprint/paper | 1.78 | Cargo Handbook (Paper Rolls) (BMT, 2025) | 2.8 | Stowage Factor Blog (Newsprint Paper Rod) (Stowage Factor Blog, 2016) |

Continued on next page

Table D.3 – continued from previous page

| **Commodity** | **Lower SF ($m^3$/tonne)** | **Lower SF source** | **Upper SF ($m^3$/tonne)** | **Upper SF source** |
|---|---|---|---|---|
| Paper articles | 1.84 | Handy Bulk (Liner Board) (HandyBulk LLC, 2025) | 9.9 | Handy Bulk (Toilet Paper) (HandyBulk LLC, 2025) |
| Printed prods. | 2.0 | Star Marine (Note Books) (Star Marine Services Ltd., 2015) | 2.7 | Star Marine (Printing Paper) (Star Marine Services Ltd., 2015) |
| Textiles/leather | 1.14 | Cargo Handbook (Textiles) (BMT, 2025) | 6.50 | Cargo Handbook (Textiles) (BMT, 2025) |
| Articles-base metal | 0.34 | Cargo Handbook (Copper Cathodes) | 1.04 | Cargo Handbook (Pipes (steel)) |
| Machinery | 4.25 | BTR (Bicycles) (Best International Transportation Co., Ltd., 2023) | 4.25 | BTR (Bicycles) (Best International Transportation Co., Ltd., 2023) |
| Electronics | 2.4 | BTR (Electric Fans) (Best International Transportation Co., Ltd., 2023) | 2.8 | BTR (Radios) (Best International Transportation Co., Ltd., 2023) |
| Motorized vehicles | 4.2 | Stowage Factor Blog (Cars) (Stowage Factor Blog, 2016) | 4.2 | Stowage Factor Blog (Cars) (Stowage Factor Blog, 2016) |
| Transport equip. | 4.2 | Stowage Factor Blog (Cars) (Stowage Factor Blog, 2016) | 4.2 | Stowage Factor Blog (Cars) (Stowage Factor Blog, 2016) |

Continued on next page

Table D.3 – continued from previous page

| **Commodity** | **Lower SF ($m^3$/tonne)** | **Lower SF source** | **Upper SF ($m^3$/tonne)** | **Upper SF source** |
|---|---|---|---|---|
| Precision instruments | 2.4 | BTR (Electric Fans) (Best International Transportation Co., Ltd., 2023) | 2.8 | BTR (Radios) (Best International Transportation Co., Ltd., 2023) |
| Furniture | 3.1 | Stowage Factor Blog (Bedsheets) (Stowage Factor Blog, 2016) | 6.23 | Stowage Factor Blog (Folding Chairs) (Stowage Factor Blog, 2016) |
| Misc. mfg. prods. | 1.6 | Stowage Factor Blog (Containers) (Stowage Factor Blog, 2016) | 3 | Stowage Factor Blog (Containers) (Stowage Factor Blog, 2016) |
| Waste/scrap | 0.8 | Handy Bulk (Steel Scrap) (HandyBulk LLC, 2025) | 2.5 | Handy Bulk (Steel Scrap) (HandyBulk LLC, 2025) |
| Mixed freight | 1.6 | Stowage Factor Blog (Containers) (Stowage Factor Blog, 2016) | 3 | Stowage Factor Blog (Containers) (Stowage Factor Blog, 2016) |
| Live animals/fish | N/A | Not estimated (excluded from this work) | N/A | Not estimated (excluded from this work) |

| **Commodity** | **SF ($m^3$/tonne)** | **Lower SF source** |
|---|---|---|
| Crude petroleum | Distribution from 1.08-1.32 | See Appendix E |
| Gasoline | 1.33 | GREET 2024 (Argonne National Laboratory, 2024) |
| Fuel oil | 1.01 | GREET 2024 (Argonne National Laboratory, 2024) |

Table D.4: Stowage factor (SF) range estimates and sources for commodities assumed to be carried by tankers.

Figures D.1 to D.3 summarize the SF ranges and tonne-mile distributions of commodities assumed to be

carried by bulk carriers, container ships, and tankers, respectively.

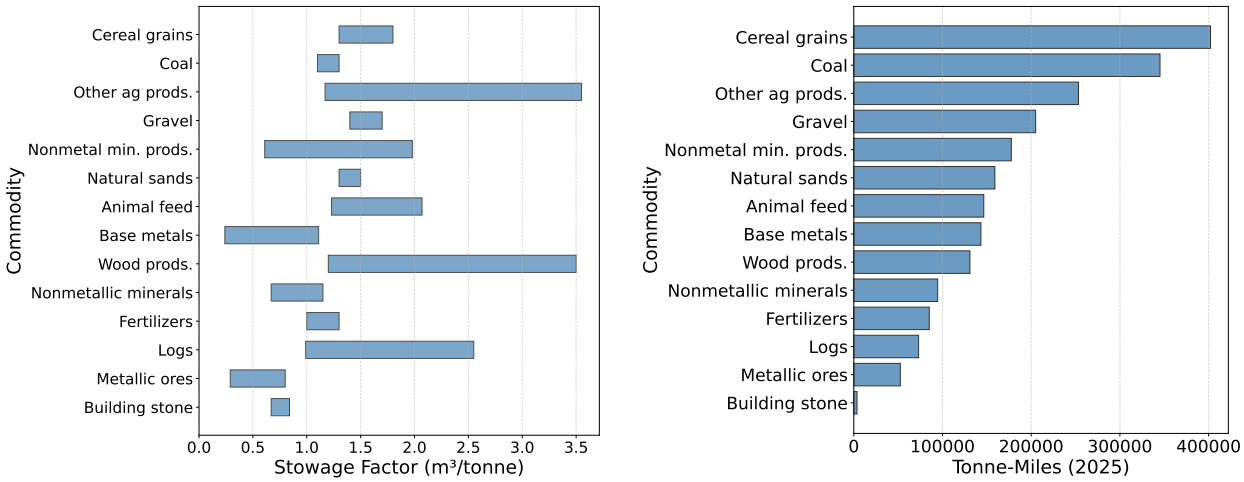


(a) Stowage Factor Ranges

(b) Tonne-miles by Commodity in 2025

Figure D.1: Left: SF ranges for each commodity assumed to be carried by bulk carriers. Right: Projected tonne-miles of each commodity carried into and out of U.S. ports in 2025 based on the FAF5 dataset.

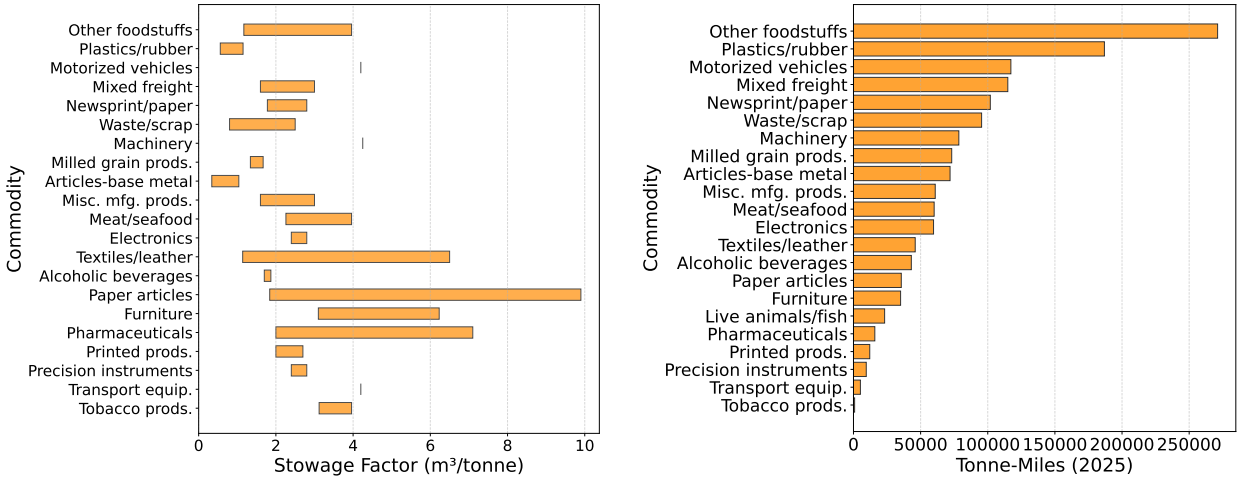


(a) Stowage Factor Ranges

(b) Tonne-miles by Commodity in 2025

Figure D.2: Left: SF ranges for each commodity assumed to be carried primarily by container ships. Right: Projected onne-miles of each commodity carried into and out of U.S. ports in 2025 based on the FAF5 dataset.

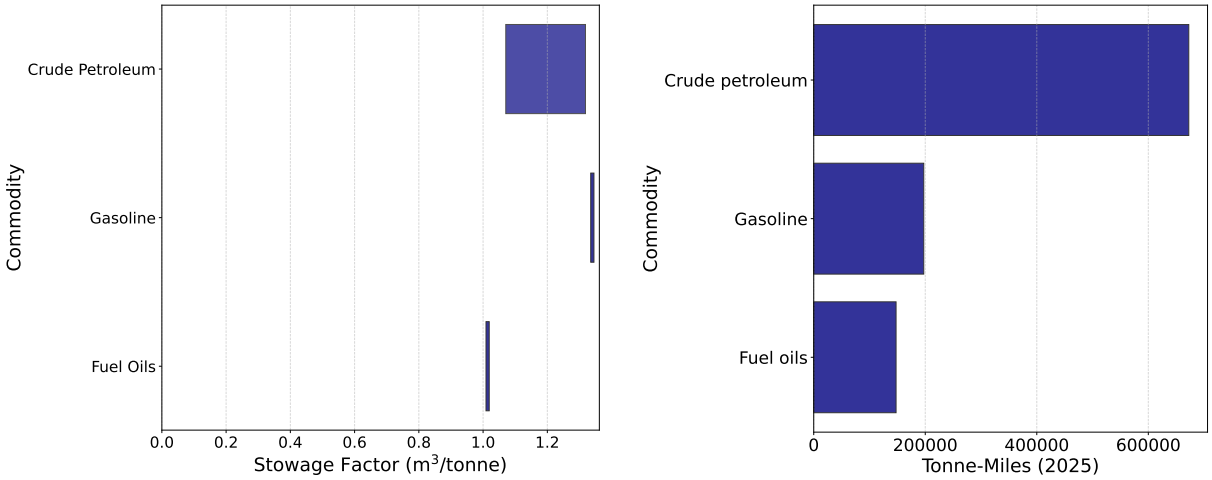


(a) Stowage Factor Ranges

(b) Tonne-miles by Commodity in 2025

Figure D.3: Left: SF ranges for each commodity assumed to be carried primarily by tanker ships. Right: Projected tonne-miles of each commodity carried into and out of U.S. ports in 2025 based on the FAF5 dataset.

# E Crude Petroleum Stowage Factor Distribution

The stowage factor distribution for crude petroleum is obtained from the average daily production of crude oil in the U.S. lower 48 states in 2023 within different density categories defined by "API gravity ranges", obtained from data published by the U.S. Energy Information Administration (2024). Fuel density $\rho^{\text{fuel}}$, in kg/L, is calculated from its API density using the standard formula (U.S. Energy Information Administration, 2025):

$$\rho^{\text{crude}} = \frac{141.5}{\text{API} + 131.5} \tag{E.1}$$

and from Equation 15, the SF is simply the inverse of the fuel density.

For API ranges with both an upper and lower bound, the central value ($\frac{\text{API}_{\text{upper}}+\text{API}_{\text{lower}}}{2}$) is used to estimate the associated fuel density using Equation E.1. For ranges provided with only an upper bound or a lower bound (eg. "55.1 or higher"), the fuel density is estimated using the provided bound:

$$\text{API}_k^{\text{central}} = \begin{cases} \dfrac{\text{API}_k^{\text{upper}} + \text{API}_k^{\text{lower}}}{2}, & \text{if } \text{API}_k^{\text{upper}} < \infty \text{ and } \text{API}_k^{\text{lower}} > -\infty \\ \text{API}_k^{\text{upper}}, & \text{if } \text{API}_k^{\text{lower}} = -\infty \\ \text{API}_k^{\text{lower}}, & \text{if } \text{API}_k^{\text{upper}} = \infty \end{cases} \tag{E.2}$$

and from Equation 15, the SF is simply the inverse of the fuel density:

$$\mathrm{SF}_k^{\text{crude, central}} = \frac{1}{\rho^{\text{crude, central}}{}_k} = \frac{\mathrm{API}_k^{\text{central}} + 131.5}{141.5} \tag{E.3}$$

A weighting factor $w_{\mathrm{SF}_k}^{\text{crude}}$ is defined for each API range $k$ based on the share of U.S. crude petroleum production in that range, and is used to scale total crude petroleum tonne-miles imported to and exported from U.S. ports, as shown in Equation 22. This assumes that production shares by API range reflect the distribution of tonne-miles for U.S. imports and exports.

$$w_{\mathrm{SF}_k}^{\text{crude}} = \frac{(\text{Average daily production})_k}{\sum_{\ell \in \text{all API ranges}} (\text{Average daily production})_\ell} \tag{E.4}$$

Table E.1 summarizes the API ranges in the EIA data, along with the assigned $\mathrm{SF}_k$, average daily crude petroleum production, and weight factor evaluated with Equation E.4 within each API range $k$. The resulting SF distribution for crude petroleum is shown in E.1.

| $\boldsymbol{k}$ | $\mathbf{API}_k^{\mathbf{lower}}$ | $\mathbf{API}_k^{\mathbf{upper}}$ | $\mathbf{SF}_k^{\mathbf{crude,central}}$ | **Production Rate (thousand barrels / day)** | $\boldsymbol{w}_{\mathbf{SF}_k}^{\mathbf{crude}}$ |
|---|---|---|---|---|---|
| 0 | $-\infty$ | 20.0 | 1.07 | 257.25 | 0.02 |
| 1 | 20.1 | 25.0 | 1.09 | 149.6 | 0.01 |
| 2 | 25.1 | 30.0 | 1.12 | 787.0 | 0.06 |
| 3 | 30.1 | 35.0 | 1.16 | 1330.4 | 0.11 |
| 4 | 35.1 | 40.0 | 1.19 | 3003.3 | 0.24 |
| 5 | 40.1 | 45.0 | 1.23 | 3766.2 | 0.30 |
| 6 | 45.1 | 50.0 | 1.26 | 2214.8 | 0.18 |
| 7 | 50.1 | 55.0 | 1.30 | 643.8 | 0.05 |
| 8 | 55.1 | $\infty$ | 120 | 344.5 | 0.03 |

Table E.1: API ranges of crude petroleum density categories defined by the EIA (U.S. Energy Information Administration, 2024). The associated central SF value, daily US production rate, and resulting weighting factor is tabulated for each density category.

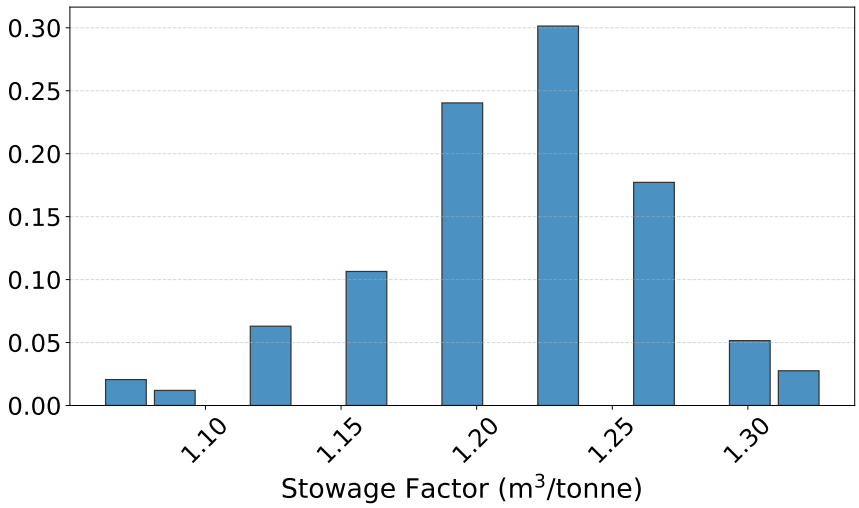


Figure E.1: Distribution of stowage factors for crude petroleum

# F Detailed Fuel and Vessel Specifications

| **Main Fuel** | Lower Heating Value $(\text{LHV})_f$ (MJ/kg) | Mass Density $\rho_f$ (kg/L) | Boil-off Rate (%/day) |
|---|---|---|---|
| Fuel oil | 39.5 (Argonne National Laboratory, 2024) | 0.991 (Argonne National Laboratory, 2024) | 0 |
| Ammonia (at -33°C) | 18.8 | 0.682 (Rumble, 2025) | 0.03 (Morgan, 2013; Al-Breiki et al., 2020) |
| Liquid Hydrogen | 120 (Argonne National Laboratory, 2024) | 0.0708 (Argonne National Laboratory, 2024) | 0.5 (Abe et al., 1998; Smith et al., 2022) |
| $CH_2$ (700 bar at 20°C) | 120 (Argonne National Laboratory, 2024) | 0.0397 (Lemmon et al., 2008) | 0 |
| Methanol | 20.1 (Argonne National Laboratory, 2024) | 0.794 (Argonne National Laboratory, 2024) | 0 |
| LNG | 48.6 (Argonne National Laboratory, 2024) | 0.428 (Argonne National Laboratory, 2024) | 0.1 (Wärtsilä, 2025) |

Table F.1: Fuel properties used in this work

| **Vessel Class** | **Vessel Size** | $P^{av}$ **(MW)** | $t^{sea}$ **(days)** |
|---|---|---|---|
| Bulk Carrier | Capesize | 10.57 | 255 |
| | Pamanax | 5.20 | 240 |
| | Handy | 3.30 | 210 |
| Tanker | 300k DWT | 19.4 | 300 |
| | 100k DWT | 10.72 | 225 |
| | 35k DWT | 6.38 | 183 |
| Container Ship | 15,000 TEU | 31.04 | 240 |
| | 8,000 TEU | 27.29 | 240 |
| | 3,500 TEU | 9.78 | 210 |
| Gas carrier | 100k CBM | 10.72 | 250 |

Table F.2: Values of powertrain-independent vessel specifications used in this work, for representative vessels defined in the NavigaTE model assumed to be built in 2025. Source: NavigaTE version 2 defaults time stamped on June 18, 2025 (Eamer et al., 2025b)

| **Main Fuel** | **Propulsion System efficiency** $\eta_f^{prop}$ | **Electrical System Efficiency** $\eta_f^{elec}$ | **Heat System Efficiency** $\eta_f^{heat}$ | **Average Combined System Efficiency** $\eta_f$ |
|---|---|---|---|---|
| Fuel oil | 52% | 50% | 82.5% | $54^{+11}_{-3}$% |
| Ammonia | 49% | 48% | 82.5% | $52^{+12}_{-3}$% |
| Hydrogen | 49% | 48% | 82.5% | $52^{+12}_{-3}$% |
| Methanol | 53% | 48% | 82.5% | $55^{+11}_{-3}$% |
| LNG | 53% | 48% | 82.5% | $56^{+11}_{-3}$% |

Table F.3: Values of powertrain-dependent vessel specifications, for representative vessels defined in the NavigaTE model assumed to be built in 2025. The reported combined system efficiency $\eta^{av}$ is averaged over all ten vessels considered in this work, and asymmetric errors shown with $^{+}_{-}$ represent the upper and lower ranges of values over all vessels. Source: NavigaTE version 2 defaults time stamped on June 18, 2025 (hydrogen defaults copied from ammonia) (Eamer et al., 2025b).

| **Fuel** | **Unit Fuel cost (2024 USD / tonne fuel)** | Fuel Production Pathway Label in Ref. (Eamer et al., 2025a) (Global Average) |
|---|---|---|
| Fuel oil | 624.50 | Fossil |
| Ammonia | 852.70 | LTE (solar) |
| $LH_2$ | 5028.59 | LTE (solar) |
| $CH_2$ | 4269.86 | LTE (solar) |
| Methanol | 1296.50 | H: LTE, C: DAC (solar) |
| LNG | 2131.50 | Fossil |

Table F.4: Unit costs of fuels used in this work, using the fuel supply chain model in Eamer et al. (2025a) - details in Section 3.6.

# References


Abe, A., M. Nakamura, I. Sato, H. Uetani, and T. Fujitani (1998). "Studies of the large-scale sea transportation of liquid hydrogen". In: *International Journal of Hydrogen Energy* 23.2, pp. 115–121. DOI: https://doi.org/10.1016/S0360-3199(97)00032-3. URL: https://www.sciencedirect.com/science/article/pii/S0360319997000323.

Ahn, Junkeon, Hwalong You, Jiheon Ryu, and Daejun Chang (2017). "Strategy for selecting an optimal propulsion system of a liquefied hydrogen tanker". In: *International Journal of Hydrogen Energy* 42.8, pp. 5366–5380. DOI: https://doi.org/10.1016/j.ijhydene.2017.01.037. URL: https://www.sciencedirect.com/science/article/pii/S0360319917300575.

Alberta Energy Regulator (2024). *Crude Oil Methodology*. URL: https://www.aer.ca/data-and-performance-reports/statistical-reports/alberta-energy-outlook-st98/crude-oil/crude-oil-methodology (visited on 12/13/2024).

Alkhaledi, Abdullah NFNR, Suresh Sampath, and Pericles Pilidis (2022). "A hydrogen fuelled LH2 tanker ship design". In: *Ships and Offshore Structures* 17.7, pp. 1555–1564. DOI: 10.1080/17445302.2021.1935626. eprint: https://doi.org/10.1080/17445302.2021.1935626. URL: https://doi.org/10.1080/17445302.2021.1935626.

American Bureau of Shipping (2021). *Hydrogen as Marine Fuel*. Tech. rep. American Bureau of Shipping. URL: https://absinfo.eagle.org/acton/attachment/16130/f-bd25832f-8a70-4cc9-b75f-3aadf5d5f259/1/-/-/-/-/hydrogen-as-marine-fuel-whitepaper-21111.pdf.

Andersen, Mads Lyder, Niels B. Clausen, and Pierre C. Sames (2013). *Costs and Benefits of LNG as Ship Fuel for Container Vessels: Key Results from a GL and MAN Joint Study*. Tech. rep. Study conducted in 2011. Germanischer Lloyd (GL) and MAN Diesel & Turbo. URL: https://www.lng-info.de/fileadmin/user_upload/studien/Studie-GL-MAN-LNG.pdf.

Argonne National Laboratory (2024). *GREET Model*. [software]. URL: https://greet.anl.gov/ (visited on 01/24/2025).

Best International Transportation Co., Ltd. (2023). *Stowage factor*. URL: https://www.exbtr.com/en/stowage.html (visited on 07/14/2025).

Best Product Solutions, Inc. (2025). *Bulk Density Guide*. URL: https://www.bpsvibes.com/bulk-density-guide (visited on 07/14/2025).

BMT (2025). *Cargo Handbook*. URL: https://www.cargohandbook.com (visited on 07/10/2025).

Al-Breiki, Mohammed and Yusuf Bicer (2020). "Technical assessment of liquefied natural gas, ammonia and methanol for overseas energy transport based on energy and exergy analyses". In: *International Journal of Hydrogen Energy* 45.60. 4th International HYDROGEN TECHNOLOGIES Congress, pp. 34927–34937. DOI: https://doi.org/10.1016/j.ijhydene.2020.04.181. URL: https://www.sciencedirect.com/science/article/pii/S0360319920315858.

Choi, Minsoo, Wongwan Jung, Sangmin Ji, and Jinkwang Lee (2025). "Optimization and analysis of reliquefaction system utilizing hydrogen as refrigerant for liquid hydrogen carriers". In: *Applied Energy* 384, p. 125490. DOI: https://doi.org/10.1016/j.apenergy.2025.125490. URL: https://www.sciencedirect.com/science/article/pii/S030626192500220X.

Dedola Global Logistics (2023). *Guide to Weight Regulations for Shipping Containers: Navigating the Ocean and Road Rules*. URL: https://dedola.com/2023/08/guide-to-weight-regulations-for-shipping-containers-navigating-the-ocean-and-road-rules/ (visited on 12/13/2024).

Demharter, Anton (1998). "Polyurethane rigid foam, a proven thermal insulating material for applications between +130°C and -196°C". In: *Cryogenics* 38.1, pp. 113–117. DOI: https://doi.org/10.1016/S0011-2275(97)00120-3. URL: https://www.sciencedirect.com/science/article/pii/S0011227597001203.

Eamer, Danika, Christopher Douglas, Sander de la Rambelje, Grace Endy, Frederik Lehn, Guiyan Zang, and Elsa Olivetti (Oct. 2025a). "Viability and Impacts of Low-carbon Fuels for Maritime Applications". In: *Proceedings of the SNAME Maritime Convention 2025*. https://www.sname.org. Society of Naval Architects and Marine Engineers (SNAME). Norfolk, VA.

Eamer, Danika, Stamatis Stamatelopoulos, and Frederik Lehn (Dec. 2025b). *Calculation and Analysis of Cargo Losses with Alternative Fuels*. Version 0.1.1. DOI: 10.5281/zenodo.18037261. URL: https://github.com/danikam/cargo-loss-code.

Federal Highway Administration (2025). *[dataset] Freight Analysis Framework (FAF5)*. URL: https://ops.fhwa.dot.gov/freight/freight_analysis/faf/ (visited on 01/24/2025).

Freight Chartering Operations (2015). *Stowage Factor of General Cargoes*. URL: https://freight-charter.blogspot.com/2015/02/stowage-factor-of-general-cargoes.html (visited on 07/10/2025).

Gómez, J., Manuel Romero-Gomez, Ramon ferreiro garcia, and A. Catoira (Jan. 2013). "On board LNG reliquefaction technology: A comparative study". In: *Polish Maritime Research* 21. DOI: 10.2478/pomr-2014-0011.

Grigorescu, Ramona, Mădălina Elena David, Lorena Iancu, P. Ghioca, and Rodica-Mariana Ion (Aug. 2019). "Waste Electrical and Electronic Equipment: A Review on the Identification Methods for Polymeric Materials". In: *Recycling* 4, p. 32. DOI: 10.3390/recycling4030032.

HandyBulk LLC (2025). *HandyBulk cargo stowage factor reference pages*. Used for bulk aggregates, fertilizer, pulpwood, logs, paper product, steel & scrap, and wheat stowage factors. URL: https://www.handybulk.com (visited on 07/14/2025).

Hintze, Mathias and Frederik Lehn (2023). *NavigaTE Explainer*. Maersk Mc-Kinney Møller Center for Zero Carbon Shipping. URL: https://cms.zerocarbonshipping.com/media/uploads/documents/NavigaTE-Explainer.pdf (visited on 01/24/2025).

Horvath, Stephen and Mahdi Fasihi (May 2018). "Techno-economic analysis of a decarbonized shipping sector: Technology suggestions for a fleet in 2030 and 2040". In: *Energy Conversion and Management* 164, pp. 230–241. DOI: 10.1016/j.enconman.2018.02.098.

International Maritime Organization (2016). *International Code for the Construction and Equipment of Ships Carrying Liquefied Gases in Bulk (IGC Code)*. 2016 Edition. London: International Maritime Organization.

International Maritime Organization (2021). "Fourth IMO GHG Study 2020: Full Report". In: URL: https://wwwcdn.imo.org/localresources/en/OurWork/Environment/Documents/Fourth%20IMO%20GHG%20Study%202020%20-%20Full%20report%20and%20annexes.pdf.

International Maritime Organization (2023). *Revised GHG reduction strategy for global shipping adopted*. URL: https://www.imo.org/en/MediaCentre/PressBriefings/pages/Revised-GHG-reduction-strategy-for-global-shipping-adopted-.aspx (visited on 01/24/2025).

Ji, Sangmin, Sejun Park, Youngkyun Seo, Minsoo Choi, and Jinkwang Lee (2025). "Design and thermodynamic evaluation of onboard NH3 BOG re-liquefaction systems for ocean-going NH3 Carriers". In: *International Journal of Refrigeration* 170, pp. 399–411. DOI: https://doi.org/10.1016/j.ijrefrig.2024.12.005. URL: https://www.sciencedirect.com/science/article/pii/S0140700724004390.

JingDong Rubber Co., LTD (2025). *What is the Density of Plain Rubber Sheet?* URL: https://www.jingdongrubber.com/what-is-the-density-of-plain-rubber-sheet/ (visited on 07/14/2025).

Kim, Kyunghwa, Gilltae Roh, Wook Kim, and Kangwoo Chun (2020). "A Preliminary Study on an Alternative Ship Propulsion System Fueled by Ammonia: Environmental and Economic Assessments". In: *Journal of Marine Science and Engineering* 8.3. DOI: 10.3390/jmse8030183. URL: https://www.mdpi.com/2077-1312/8/3/183.

Klebanoff, L.E., J.W. Pratt, and C.B. LaFleur (2017). "Comparison of the safety-related physical and combustion properties of liquid hydrogen and liquid natural gas in the context of the SF-BREEZE high-speed fuel-cell ferry". In: *International Journal of Hydrogen Energy* 42.1, pp. 757–774. DOI: https://doi.org/10.1016/j.ijhydene.2016.11.024. URL: https://www.sciencedirect.com/science/article/pii/S036031991633316X.

Klell, Manfred (2010). "Storage of Hydrogen in the Pure Form". In: *Handbook of Hydrogen Storage*. John Wiley & Sons, Ltd. Chap. 1, pp. 1–37. DOI: https://doi.org/10.1002/9783527629800.ch1. eprint: https://onlinelibrary.wiley.com/doi/pdf/10.1002/9783527629800.ch1. URL: https://onlinelibrary.wiley.com/doi/abs/10.1002/9783527629800.ch1.

Korberg, A.D., S. Brynolf, M. Grahn, and I.R. Skov (2021). "Techno-economic assessment of advanced fuels and propulsion systems in future fossil-free ships". In: *Renewable and Sustainable Energy Reviews* 142, p. 110861. DOI: https://doi.org/10.1016/j.rser.2021.110861. URL: https://www.sciencedirect.com/science/article/pii/S1364032121001556.

Krikkis, Rizos N. (2018). "A thermodynamic and heat transfer model for LNG ageing during ship transportation. Towards an efficient boil-off gas management". In: *Cryogenics* 92, pp. 76–83. DOI: https://doi.org/10.1016/j.cryogenics.2018.04.007. URL: https://www.sciencedirect.com/science/article/pii/S0011227518300717.

Lemmon, Eric W., Marcia L. Huber, and Jacob W. Leachman (2008). "Revised Standardized Equation for Hydrogen Gas Densities for Fuel Consumption Applications". In: *Journal of Research of the National Institute of Standards and Technology* 113.6, pp. 341–350. DOI: 10.6028/jres.113.028. URL: https://doi.org/10.6028/jres.113.028.

Maersk Mc-Kinney Møller Center for Zero Carbon Shipping (Sept. 2022). *Preparing Container Vessels for Conversion to Green Fuels*. Tech. rep. Accessed: 2025-07-02. Maersk Mc-Kinney Møller Center for Zero Carbon Shipping. URL: https://www.zerocarbonshipping.com/publications/preparing-container-vessels-for-conversion-to-green-fuels.

Maersk Mc-Kinney Møller Center for Zero Carbon Shipping (Sept. 2023). *Concept design of a 15,000 TEU ammonia-fueled container vessel*. Tech. rep. Accessed: 2025-07-02. Maersk Mc-Kinney Møller Center for Zero Carbon Shipping. URL: https://www.zerocarbonshipping.com/publications/concept-design-of-a-15-000-teu-ammonia-fueled-container-vessel.

Maersk Mc-Kinney Møller Center for Zero Carbon Shipping (Oct. 2024a). *Emerging ship design principles for ammonia-fueled vessels*. Tech. rep. Accessed: 2025-07-02. Maersk Mc-Kinney Møller Center for Zero Carbon Shipping. URL: https://www.zerocarbonshipping.com/publications/emerging-ship-design-principles-for-ammonia-fueled-vessels.

Maersk Mc-Kinney Møller Center for Zero Carbon Shipping (July 2024b). *Preparing Tanker Vessels for Conversion to Green Fuels*. Tech. rep. Accessed: 2025-07-02. Maersk Mc-Kinney Møller Center for Zero Carbon Shipping. URL: https://www.zerocarbonshipping.com/publications/preparing-tanker-vessels-for-conversion-to-green-fuels.

Maersk Mc-Kinney Møller Center for Zero Carbon Shipping (June 2025). *Concept design of a 3,500 TEU ammonia-fueled container vessel*. Tech. rep. Maersk Mc-Kinney Møller Center for Zero Carbon Shipping. URL: https://www.zerocarbonshipping.com/publications/concept-design-of-a-3-500-teu-ammonia-fueled-container-vessel (visited on 07/02/2025).

Mao, Xiaoli, Dan Rutherford, Liudmila Osipova, and Bryan Comer (Mar. 2020). *Refueling Assessment of a Zero-Emission Container Corridor Between China and the United States: Could Hydrogen Replace Fossil Fuels?* Working Paper. Accessed: 2025-07-02. International Council on Clean Transportation (ICCT). URL: https://theicct.org/publication/refueling-assessment-of-a-zero-emission-container-corridor-between-china-and-the-united-states-could-hydrogen-replace-fossil-fuels/.

Maritime Brokers and Consultants, Inc. (2024). *Ships we work with*. URL: https://www.marbrokers.com/ship-we-work-with (visited on 12/13/2024).

Mooney, Christopher (1997). *Monte Carlo Simulation*. Thousand Oaks, California: SAGE Publications, Inc. DOI: 10.4135/9781412985116. URL: https://methods.sagepub.com/book/mono/monte-carlo-simulation/toc.

Morgan, Eric R. (2013). "Techno-Economic Feasibility Study of Ammonia Plants Powered by Offshore Wind". PhD thesis. University of Massachusetts Amherst.

Qu, Yongfeng, Ibrahima Noba, Xiaochun Xu, Romain Privat, and Jean-Noël Jaubert (2019). "A thermal and thermodynamic code for the computation of Boil-Off Gas – Industrial applications of LNG carrier". In: *Cryogenics* 99, pp. 105–113. DOI: https://doi.org/10.1016/j.cryogenics.2018.09.002. URL: https://www.sciencedirect.com/science/article/pii/S0011227518301358.

Rivard, Etienne, Michel Trudeau, and Karim Zaghib (2019). "Hydrogen Storage for Mobility: A Review". In: *Materials* 12.12. DOI: 10.3390/ma12121973. URL: https://www.mdpi.com/1996-1944/12/12/1973.

Rumble, John R., ed. (2025). *CRC Handbook of Chemistry and Physics*. 106th ed. Internet Version 2025. Boca Raton, FL: CRC Press/Taylor & Francis.

Smith, Jessie R., Savvas Gkantonas, and Epaminondas Mastorakos (2022). "Modelling of Boil-Off and Sloshing Relevant to Future Liquid Hydrogen Carriers". In: *Energies* 15.6. DOI: 10.3390/en15062046. URL: https://www.mdpi.com/1996-1073/15/6/2046.

Star Marine Services Ltd. (2015). *Stowage factors*. URL: https://www.starmarine.net/stowage-factor/ (visited on 07/14/2025).

Stolz, Benedikt, Martin Held, Gabriel Georges, and et al. (2022). "Techno-economic analysis of renewable fuels for ships carrying bulk cargo in Europe". In: *Nature Energy* 7, pp. 203–212. DOI: 10.1038/s41560-021-00957-9. URL: https://doi.org/10.1038/s41560-021-00957-9.

Stowage Factor Blog (2016). *Stowage factor for all cargoes: Dry Bulk Stowage Factor*. URL: https://stowagefactor.blogspot.com/2016/09/dry-bulk-stowage-factor.html (visited on 07/14/2025).

U.S. Department of Energy (2013). *Liquefied Natural Gas: Understanding the Basic Facts*. U.S. Department of Energy. URL: https://www.energy.gov/sites/prod/files/2013/04/f0/LNG_primerupd.pdf (visited on 12/13/2024).

U.S. Energy Information Administration (2024). *Crude Oil and Lease Condensate Production by API Gravity*. URL: https://www.eia.gov/dnav/pet/pet_crd_api_adc_mbblpd_m.htm (visited on 03/20/2025).

U.S. Energy Information Administration (2025). *Petroleum and Other Liquids: Definitions, Sources and Explanatory Notes*. URL: https://www.eia.gov/dnav/pet/tbldefs/pet_pnp_crq_tbldef2.asp (visited on 07/15/2025).

Wärtsilä (2020). *Compact Reliq™ BOG Reliquefaction Unit*. Tech. rep. © 2020 Wärtsilä Corporation. WÄRTSILÄ® is a registered trademark. Wärtsilä Corporation. URL: https://www.wartsila.com/docs/default-source/product-files/ogi/lng-solutions/compact-reliq-bog-reliquefaction.pdf?sfvrsn=fbf0ba44_8.

Wärtsilä (2025). *Wärtsilä Marine Encyclopedia: Boil-off Rate (BOR)*. URL: https://www.wartsila.com/encyclopedia/term/boil-off-rate-(bor) (visited on 07/02/2025).